COOPERATIVE NATIONAL PARK RESOURCES STUDIES UNIT
UNIVERSITY OF HAWAII AT MANOA

Department of Botany
3190 Maile Way
Honolulu, Hawaii 96822
(808) 956-8218

Technical Report 92

ELEVATIONAL PATTERNS OF CLIMATE ON THE LEEWARD SLOPE OF EAST MAUI, HAWAII

William P. Minyard, Thomas W. Giambelluca and Dennis Nullet

Department of Geography
University of Hawai'i at Manoa,
Honolulu, HI 96822

Cooperative Agreement
CA 8032-2-0001

February 1994

TABLE OF CONTENTS

LIST OF TABLES ii
LIST OF FIGURES ii
INTRODUCTION 1
METHODS 1
RESULTS
MONTHLY AVERAGES 2
ELEVATION EFFECTS 2
ANNUAL CYCLE 4
DIURNAL CYCLE 6
APPLICATIONS
ANALYSIS OF CLIMATIC EXTREME EVENTS 8
POTENTIAL EVAPORATION 9
DISCUSSION 10
BIBLIOGRAPHY 12

LIST OF TABLES

1. Monthly Averages of Climate Measurements Along Climate Transect 13
2. Elevational Patterns of Climate Along Climate Transect 18
3. Annual Climate Pattern Along Climate Transect 19
4. Diurnal Climate Pattern Along Climate Transect 21

LIST OF FIGURES

1. Map of the Study Area 24
2. Monthly Mean Net Radiation 25
3. Monthly Mean Global Radiation 25
4. Monthly Mean Air Temperature 26
5. Monthly Mean Relative Humidity 26
6. Monthly Mean Vapor Pressure 27
7. Monthly Mean Wind Speed 27
8. Monthly Mean Soil Heat Flux 28
9. Monthly Mean Rainfall 28
10. Monthly Mean Atmometer Evaporation 29
11. Annual Mean Solar Radiation 29
12. June-July Mean Solar Radiation 30
13. December-January Mean Solar Radiation 30
14. Cloud Attenuation of Global Radiation 31
15. Mean Air Temperature 31
16. Mean Relative Humidity 32
17. Mean Vapor Pressure 32
18. Mean Wind Speed 33
19. Mean Soil Heat Flux 33
20. Annual Mean Rainfall 34
21. Seasonal and Annual Rainfall Along Climate Station Transect 34
22. Annual Mean Atmometer Evaporation 35
23. Annual Cycle of Net Radiation 35
24. Annual Cycle of Global Radiation 36
25. Annual Cycle of Air Temperature 36
26. Annual Cycle of Relative Humidity 37
27. Annual Cycle of Vapor Pressure 37

28. Annual Cycle of Wind Speed 38
29. Annual Cycle of Soil Heat Flux 38
30. Annual Cycle of Rainfall 39
31. Annual Cycle of Atmometer Evaporation 39
32. Annual Cycle of Rainfall Versus Atmometer Evaporation at 950 meters Elevation 40
33. Annual Cycle of Rainfall Versus Atmometer Evaporation at 1650 meters Elevation 40
34. Annual Cycle of Rainfall Versus Atmometer Evaporation at 2130 meters Elevation 41
35. Annual Cycle of Rainfall Versus Atmometer Evaporation at 2600 meters Elevation 41
36. Annual Cycle of Rainfall Versus Atmometer Evaporation at 3000 meters Elevation 42
37. Mean Diurnal Cycle of Net Radiation 42
38. Mean Diurnal Cycle of Global Radiation 43
39. Mean Diurnal Cycle of Air Temperature 43
40. Mean Diurnal Cycle of Relative Humidity 44
41. Mean Diurnal Cycle of Vapor Pressure 44
42. Mean Diurnal Cycle of Wind Speed 45
43. Mean Diurnal Cycle of Soil Heat Flux 45
44. Mean Diurnal Cycle of Rainfall 46
45. Mean Diurnal Cycle of Atmometer Evaporation 46
46. Relative Humidity and Rainfall During Snowstorm of January 14-15, 1992 47
47. Air and Ground Temperatures During Snowstorm of January 14-15, 1992 47
48. Net and Global Radiation During Snowstorm of January 14-15, 1992 48
49. Diurnal Pattern of Atmometer Measurements Versus Potential Evaporation Estimates at 950 meters Elevation 48
50. Diurnal Pattern of Atmometer Measurements Versus Potential Evaporation Estimates at 1650 meters Elevation 49
51. Diurnal Pattern of Atmometer Measurements Versus Potential Evaporation Estimates at 2130 meters Elevation 49
52. Diurnal Pattern of Atmometer Measurements Versus Potential Evaporation Estimates at 2600 meters Elevation 50
53. Diurnal Pattern of Atmometer Measurements Versus Potential Evaporation Estimates at 3000 meters Elevation 50

ABSTRACT

The climate of the main Hawaiian islands is strongly influenced by persistent subsidence inversion and trade winds characteristic of the region. In the middle and upper elevations of the high volcanic peaks climate is directly affected by the presence and movement of this inversion. Five climate stations have been operating on an altitudinal transect between 950 meters and 3000 meters elevation on the leeward side of East Maui in order to measure and describe the climate zones created by the inversion layer. Hourly measurements of solar radiation, net radiation, air temperature, relative humidity, wind, rainfall and atmometer evaporation were made. This report documents the results of these measurements in terms of elevational, annual and diurnal patterns, as well as addressing some aspects of climate variability and the applications of this data in estimating rates of potential evapotranspiration. This report summarizes two to three years of data from these climate stations and can be used as a reference for future research on the relationship between native ecosystems and climate within the area of study.

INTRODUCTION

The climate of the main Hawaiian islands is strongly influenced by the persistent subsidence inversion and northeasterly trade winds characteristic of the region. The inversion layer and trade winds account for much of the spatial distribution of climate in Hawaii. Trade winds bring in moist oceanic air which blows up the mountains, cools adiabatically to the dew point, then forms clouds and rain on the windward sides of the islands. On the leeward side descending drier air warms adiabatically creating a rain shadow effect. This orographic rainfall pattern is modified by the subsidence inversion layer which exists at an average altitude of about 2000 meters (Riehl *et al.* 1951) and acts as a barrier to the further upward movement of clouds. Hence the climate above the inversion begins to become much drier with increased elevation.

Riehl *et al.* (1951) described 4 atmospheric layers over the ocean in the vicinity of Hawaii: subcloud, cloud, inversion and free atmosphere. The subcloud layer extends from sea level to about 600 to 800 meters, at which point the well-mixed atmosphere is saturated with water vapor and clouds are found. This cloud layer extends up to the bottom of the inversion layer at about 2000 meters. The inversion layer has a thickness of about 400 meters, and above 2400 meters is the dry stable air of the free atmosphere. Because of the loss of water through rainfall, heating from the land, and downmixing of dry air the bottom of the cloud layer over land is considerably higher than the 600-800 meter height over the open ocean (Lavoie 1974).

Palinologist Otto Selling (1948) analyzed bog cores from West Maui, Kauai and Molokai and found that significant changes in plant community structure have occurred through time in these locations. These changes are indicative of large and long-term changes in rainfall amounts in places which are now among the wettest on earth, and can reasonably be interpreted to mean that the average inversion layer height has fluctuated in the past by at least 600 meters (Selling 1948). Based on comparison with palinological data elsewhere, Selling concluded that the inversion layer was lower during colder periods and higher during warmer periods than the present. If this is the case, then the prospects for the future with carbon dioxide induced global warming involve a higher average inversion layer height with accompanying increases in rainfall and cloudiness at locations in Hawaii above 2000 meters. These potential climatic changes could have serious negative consequences for the native Hawaiian biota at high altitudes which has adapted to the current climates but is in competition with newly introduced exotic species.

METHODS

In order to study the elevational pattern of climate, five climate stations were installed between 950 and 3000 meters elevation on the western slope of East Maui, with the first instruments set up in June of 1988 (Figure 1). With minor exceptions, instruments have been recording continuous hourly data at all five stations since April, 1990. About 2 to 4 years of hourly average data have been collected at these five stations for global and net radiation, air temperature, relative humidity, wind speed, soil heat flux, rainfall and potential evaporation using an automated atmometer described by Giambelluca *et al.* (1992).

Global radiation was measured at each site with Eppley precision pyranometers, which were maintained level through weekly servicing. Net radiation was measured with Fritschen type net radiometers located above the canopy, also leveled weekly. Air temperature and relative humidity were measured with Vaisala HMD 30YB instruments at a height of 2 meters above the ground. Wind speed was measured with cup anemometers placed 2 meters above the ground. Soil heat flux was measured with transducer plates placed approximately 3 cm below the soil surface. Rainfall was measured with 0.01" sensitivity tipping bucket rain gauges, which were cleaned weekly or biweekly. All instruments were connected to a Li-Cor datalogger which took minutely readings and recorded hourly average values from these readings.

Data from the climate stations was stored on a computer hard drive, and visual inspection of graphed data in conjunction with notes from the field was used to screen out anomalous data. Global radiation data was additionally calibrated so that the clearest days at each station corresponded to the calculated clear day global radiation values as determined by the model of Bird and Riordian (1986). Soil heat flux data was adjusted so that yearly mean values would equal zero by adding or subtracting a constant from all data. For further analysis, a mean diurnal pattern was obtained for each instrument and month from the beginning of

the instrument's operation, and this data was used to compute annual, monthly and diurnal means. For long-term rainfall means, three additional stations were used. The long-term station at 2130 meters had 40 years of continuous data and was used as the baseline station. The long-term summit station had 10 years of data and the long-term station at 950 meters had 8 years of data. Linear regression equations were determined relating yearly rainfall at each of these two stations to the station at 2130 meters, and these equations were used to adjust the two stations to a common 40 year base period from 1949-1988.

RESULTS

MONTHLY AVERAGES

Figures 2-10 and Table 1 present the average values for each instrument and month and the calculated average vapor pressure. The spatial and temporal trends found in these graphs will be analyzed in more detail in separate discussions. However, some characteristics of the data are revealed in these graphs which are relevant to the descriptions of spatial and temporal patterns.

Of particular importance is the length of record for the data. Global and net radiation instruments have been set up for the longest period along the transect and have been recording almost continuously at the lower three stations since June of 1988. The rest of the instruments for these stations have been operating more or less continuously since October, 1989 and the two upper stations have been operating since March, 1990. Hence for most of the data there is about a 2 to 2.5 year record. This record is long enough to discern general spatial and temporal patterns, but is too short too allow more specific conclusions about long-term means and patterns - particularly with highly variable data such as rainfall.

Another result of the shortness of the record is that single events or unusual patterns can skew the data from what might be represented with a longer period of record. For this data, the months of November, 1990 and January, 1991, represented interesting departures from the expected mean patterns of cloudiness and rainfall. A number of winter storms struck in the winter of 1990-1991, bringing above-average rainfall to high elevation areas. Additionally, these storms brought significantly more recorded rainfall to the station at 3000 meters than to the station at 2130 meters during this time (Figure 9). This elevation distribution contrasts with data available from long-term rainfall records and clearly should be interpreted with caution. January, 1991 was a particularly unusual month, recording moderate to high rainfall at the high elevation stations but also recording some of the clearest, driest weather for the period of record (Figures 5 and 6).

As has been indicated, short-term variability in weather patterns preclude detailed discussion of long-term climate patterns. However, this variability itself is an important climate factor which can be addressed in greater detail through this data. Some climate factors such as net and global radiation (Figures 2 and 3), air temperature (Figure 4) and wind speed (Figure 7) exhibit relatively stable spatial and temporal patterns at all of the climate stations. Other factors such as relative humidity (Figure 5) seem to maintain relatively consistent spatial patterns but have a lot of temporal variability at 2130 meters and above. Rainfall (Figure 9) is highly variable both temporally and spatially, although the annual pattern is still evident from the current data set.

Atmometer evaporation, one of the more interesting measurements at these climate stations, is influence by a variety of meteorological factors including net radiation, relative humidity, air temperature and wind speed. The variability in all of these factors combine to create a great deal of short-term spatial and temporal variability in atmometer evaporation as well (Figure 10).

ELEVATION EFFECTS

Table 2 gives values used in Figures 11 through 20 and 22. In Figures 11-13, estimated clear sky global radiation is shown for comparison with measured global and net radiation. In annual measurements (Figure 11), measured global and net radiation are lowest at the 1650 meter station and are higher above and below this station. Above 1650 meters, global and net radiation generally increase with elevation to maximum values at 3000 meters. Summer and winter patterns are similar to the annual pattern, with summer radiation greater than and winter radiation less than annual averages (Figures 12 and 13).

Comparing global radiation with clear sky values in Figure 14 shows an annual average cloud

attenuation of insolation as high as 47% at 1650 meters elevation, with less attenuation above and below. At 950 meters, cloud attenuation averages 37% for the year. This station on the low flank of the volcano is well below and beyond the bottom of the cloud layer which often forms around the volcano in the early afternoon, hence it has lower cloud attenuation of global radiation than the station at 1650 meters which is most often in the cloud layer. Above 1650 meters cloud attenuation of global radiation decreases with elevation, reaching 29%, 21% and 15% of global radiation at 2130 meters, 2600 meters and 3000 meters elevation respectively.

In general, cloud attenuation of global radiation is higher at all elevations in the summer than in the winter, except at the summit which has greater winter cloudiness. Except for at the summit, this is counter to what might be expected based on the tendency for a weaker winter inversion and winter storms to increase cloudiness at upper elevations. Perhaps greater mountain heating in summer months is enough to generate greater cloudiness up to 2600 meters, or perhaps the unusually clear and rainless month of January, 1991 is skewing the results from what would normally be expected to occur.

As can be seen in Table 1, net radiation as a percentage of global radiation is quite similar between the lower three stations, ranging from 57% to 59% in the summer and 51% to 55% in the winter. The highest elevation station has slightly higher net radiation as a percentage of global radiation, at 64% in the summer and 58% in the winter. The station at 2600 meters exhibited the greatest range in net radiation as a percent of global radiation at 56% in the summer and 44% in the winter. For all stations, net radiation is a lower percentage of global radiation in the winter than in the summer. Winter low net radiation at 2600 meters relative to nearby stations is not easily explainable and could be due to problems with instrument calibration, although the effects of seasonal changes in vegetation cannot be ruled out.

While no inverse temperature lapse rate is seen in the mean profiles (Figure 15), the inversion's influence is apparent in the reduced temperature gradient between 1650 meters and 2600 meters. From 950 meters to 1650 meters the temperature lapse rate averages 0.0059 °C/m for the year, differing only slightly between summer (0.0056 °C/m) and winter (0.0053 °C/m). Between 2600 and 3000 meters the lapse rate is quite similar, averaging 0.0058 °C/m in the summer, winter and yearly averages. From 1650 meters to 2600 meters, however, the annual lapse rate averages only 0.0026 °C/m or less than half the lapse rates above 2600 meters and below 950 meters.

Within this inversion layer zone between 1650 and 2600 meters, the average height of the inversion layer appears to occur more often in the upper part of this zone. Between 2130 meters and 2600 meters the average lapse rate is lowest for the entire transect at 0.0023 °C/m. Between 1650 meters and 2130 meters the average lapse rate is 0.0029 °C/m, still indicating the effects of the inversion layer, but to a lesser degree.

The greater persistence of the inversion layer in summer versus winter months can be discerned from this data. Between 1650 meters and 2600 meters the lapse rate averages 0.0024 °C/m in the summer months and 0.0026 °C/m in the winter months. This effect is small, but more pronounced between 1650 and 2130 meters in which the lapse rate is 0.0027 °C/m in the summer and 0.0031 °C/m in the winter.. Between 2130 meters and 2600 meters the summer lapse rate is equal to the winter lapse rate at 0.0021 °C/m. These temperature profiles indicate that in general the inversion layer is more often found between 2130 meters and 2600 meters than between 1650 meters and 2130 meters, and that the inversion is slightly more persistent in the summer than the winter.

In general, relative humidity decreases with elevation through the transect, from an annual mean high of 83% at 950 meters to only 44% at 3000 meters (Figure 16). Summer is higher than winter relative humidity at all stations. This annual pattern agrees with the annual pattern of greater summer versus winter cloudiness at all but the highest station, and indicates that this pattern is not simply an artifact of the instrument calibration. Relative humidity at 1650 meters in particular seems to reflect greater summer cloudiness with summer relative humidity at this elevation higher than relative humidity at 950 meters.

Because relative humidity is influenced by both temperature and water content of the air, vapor pressure profiles (Figure 17) differ somewhat from relative humidity profiles. In both summer and winter months as well as annual averages, vapor pressure decreases nearly linearly with elevation.

Summer months with higher average temperatures and relative humidity have higher vapor pressure than winter months.

Wind speed is greatly influenced by local topography and instrument exposure. Despite these site-specific influences, it is apparent from Figure 18 that average wind speed increases with elevation both in winter and summer. The only exception is at 2600 meters in the summer which has somewhat lower wind speed than 2130 meters. The presence of a strong inversion layer between these elevations could be in part responsible for this exception, with relatively calm conditions being associated with the inversion layer boundary. In general, wind speed is greater in winter than in the summer. This difference seems to be most prominent at the three middle-elevation stations at 1650, 2130 and 2600 meters. Perhaps the presence of a stronger summer inversion is also responsible for this effect, preventing summer diurnal winds from moving up and down the mountain across the inversion layer.

Soil heat flux measurements indicate an interesting, if not easily explainable pattern between summer and winter extremes (Figure 19). Four of the five stations exhibit the expected pattern of positive net soil heat flux in summer months and negative flux in winter months. The exception is at 2600 meters at which winter flux is slightly higher than summer flux. The general shape of the graph indicates that the annual range of soil heat flux is greatest at the summit, is lower at the three intermediate stations, and increases again at the lowest station. It seems quite possible that this pattern is an artifact of instrument error, since the range in net radiation at 2600 meters should reasonably produce the opposite effect in soil heat flux from what it did.

Rainfall is notoriously variable from year to year, so conclusions about spatial patterns cannot be adequately drawn from the current data set. Nonetheless, some patterns which accord with long-term normals can be seen in the data (Figures 20 and 21). At all stations, winter rainfall was substantially higher than summer rainfall. In both winter and summer the lower stations had lower rainfall than the middle station at 2130 meters. Additionally, most of the seasonal rainfall indicates that the station at 2130 meters receives the maximum rainfall for the transect. Above this station the inversion layer exerts a negative influence on rainfall and below this elevation the rain shadow effect of the mountain exerts an increasing influence. The winter of 1990-91 indicates that rainfall is highest at the summit, but this data does not accord with long-term normals and should be interpreted with caution. As a result of the winter of '90-'91 the annual pattern of rainfall appears greater at the summit than long term normals indicate. The winter of 1991-92 had a rainfall pattern which more closely fit the long-term pattern. Because of the high variability of rainfall, this limited data set must be interpreted with caution in terms of absolute values and spatial patterns of rainfall normals.

As can be seen in Figure 22, atmometer evaporation is highly spatially variable through the climate station transect. Atmometer evaporation is a measure of the maximum amount of evaporation which would occur of water were unlimited in the soil. It is driven by net radiation, but is influenced by relative humidity, air temperature and wind speed as well. Despite this complex of factors, it appears that annual mean atmometer evaporation rates are quite similar at the three lower sites at 950, 1650 and 2130 meters elevation. Above 2130 meters there is a sharp gradient of increasing atmometer evaporation with elevation, such that the station at 3000 meters experiences average rates 79% higher than at 2130 meters. Seasonal variations are generally as would be expected, with summer values between 1.3 and 2.1 mm/day higher than winter values at all stations except at 1650 meters. At this station, relatively high summer cloudiness (Figure 14) and relative humidity (Figure 16) as compared to winter values act to limit the annual range to only about 0.1 mm/day.

ANNUAL CYCLE

The annual cycle for each measured value is given in Table 3 and Figures 23 through 31. The annual cycles of net and global radiation (Figures 23 and 24) are indicative of the march of solar declination and day length as well as cloud cover variations related to season. Cloud cover probably has significant interannual variability, and thus these measurements represent a small sample which might not be completely representative of long term means. Nevertheless, the general patterns of insolation and radiation balance are apparent. The maximum of global radiation occurs in May for two stations and in June for the other three stations. The annual net radiation peak occurs in May at one station, June at three stations and July at one

station. Solar radiation minimums occur in November at 3000 meters and in December for the other four stations. The 3000 meter minimum is probably due to the influence of November 1990, which was unusually cloudy and rainy. Net radiation minimums occurred in December for all five stations.

The spatial pattern of solar and net radiation is again evident in the annual cycle, with both solar and net radiation consistently higher at higher elevations. Additionally, the magnitude of the annual cycle appears to be greater at higher elevations. The station at 1650 meters consistently records the lowest values of solar and net radiation as well as the least difference between summer and winter radiation, probably as a result of the clouds often found at this elevation.

The small annual temperature cycle typical of marine tropical climates can be seen in Figure 25. The coldest month averages 4.0, 4.1, 3.2, 3.5, and 3.9 °C colder than the warmest month for the stations at 950, 1650, 2130, 2600 and 3000 meters respectively. Temperature maximums occur in August for 4 of the 5 stations and in September at 950 meters. Temperature minimums occur in February for 2 stations and in March for the other 3 stations. Hence the annual cycle of temperature lags about 2-3 months behind the annual cycles of global and net radiation.

Mean annual cycles of relative humidity appear to be dependent on elevation along the transect, as can be seen in Figure 26. The greater persistence of the inversion layer in summer months can be seen in the strong gradient of decreasing relative humidity with increasing elevation above the 1650 meter station during this time. Fall and winter months on average have a consistent but weaker gradient of decreasing relative humidity with increasing elevation. At 950 meters relative humidity remains quite constant throughout the year, averaging between 83% and 86% for all months except January. This results from the constant mixing of air at this elevation with air in contact with the ocean surface. At 1650 meters a slight annual pattern appears, with summer relative humidity between 83% and 86% versus winter values below 75%. Excluding the anomalous month of January, the upper 4 stations seem to have a quasi annual cycle of relative humidity, with peaks in the fall and lows in the spring. Because of the shortness of the record, these patterns should be interpreted with caution. The relatively low January values of relative humidity at all stations corresponds to an unusual month with relatively low rainfall and clear skies. With a longer record, these fluctuations would exert less influence and the typical pattern would become more evident.

Vapor pressure is related to both temperature and relative humidity (Figure 27). The annual pattern of vapor pressure appears quite similar to the temperature pattern, with local maximum values in September for all stations. The annual cycle appears less pronounced at higher stations where high temperatures in the summer generally occur coterminously with low relative humidity.

Annual patterns of wind speed also appear to depend on elevation (Figure 28). At the 950 meter station as well as the 3000 meter station, there is no obvious annual pattern of wind speed. At the 1650, 2130 and 2600 meter stations, however, a distinct annual pattern occurs with generally higher winter winds than summer.

Annual soil heat flux generally accords with expected patterns related to net radiation (Figure 29 and 23). The largest annual cycle occurs at 3000 meters, which also has the largest annual cycles of net radiation and air temperature. The pattern at 2600 meters is unusual with a maximum in January and a minimum in September, and is probably a result of problems with the instrument. An annual pattern is evident at the three lower stations, with the station at 1650 meters recording the lowest annual range and the station at 950 meters recording the greatest annual range of these three.

Monthly mean values of rainfall are plotted in Figure 30. Values during the winter are highly dependent on the timing and intensity of individual storms for this short period of record, hence only the broadest inferences can be made about long-term means. Additionally, problems with instrument malfunction can produce spurious results. Nonetheless, rainfall at all stations exhibits the annual pattern characteristic of the leeward sides of the Hawaiian islands. The large majority of the rainfall during this short period of record occurred during the season from November to March. Additionally, it appears that summer rainfall was limited at all stations but was substantially higher at 2130 meters than at the other stations, which accords with the long term record.

Monthly means of atmometer evaporation are plotted in Figure 31. It is highest along the transect

at the upper two stations because of the low relative humidity, high net radiation and high mean wind speeds. The large range in annual net radiation and relative humidity at the upper two stations also contribute the large range in annual atmometer evaporation at these stations. The stations at 2130 and 950 meters also exhibit annual patterns, but with lower average values due to the relatively more moist air at these locations. At 1650 meters little annual pattern is evident. This can be explained by the relatively shallow cycle of net radiation at this elevation in combination with an annual cycle of relative humidity which counteracts the net radiation cycle.

Soil moisture is an important environmental variable for plants, and depends on a great deal of factors including soil properties, hill slope angle, rainfall amounts and evapotranspiration from plants and the soil. As a first step towards describing water availability for plants, the annual pattern of rainfall was plotted along with the annual pattern of atmometer evaporation at each station. As can be seen in Figures 32-36, each location along the transect has its own annual pattern of water availability. The data at the 950 meter station indicate that this location is quite dry (Figure 32). This location has the longest period of dry weather of all the stations with a rainfall deficit (defined here as monthly average atmometer evaporation minus rainfall) for 10 months of the year. The rainfall deficit in the summer months reaches up to 4.1 mm/day and averages 3.0 mm/day. At 1650 meters, the summer period of rainfall deficit is less extreme than at 950 meters, lasting for 9 months with a maximum deficit of 3.2 mm/day and an average of 1.8 mm/day (Figure 33). At 2130 meters, the dry summer is mild compared to 950 meters, with a length of only 4 months, a maximum deficit of 3.7 mm/day and an average deficit of 2.9 mm/day (Figure 34).

Above 2130 meters, rapid rates of evaporation produce substantial summer water deficits. At 2600 meters, the period of water deficit lasts for 7 consecutive months, has a maximum of 5.8 mm/day and averages 4.0 mm/day (Figure 35). At 3000 meters the summer dry season lasts for 7 months, has a maximum of 7.5 mm/day and averages 5.5 mm/day (Figure 36). Although this method of assessing potential water stress on plants is far from perfect, it does give an indication of the relative water stresses between different locations on the transect. Clearly the very high summer atmometer evaporation rates and low rainfall at high elevations contribute to making this area quite desert like in summer months. The loose cinder soil probably acts synergistically with the climate in this respect.

From these comparisons it can be seen that the environment above the temperature inversion layer is quite different from that below with respect to water availability for vegetation. Just below the top of the inversion layer on the leeward side is an area of relatively mild climate from the perspective of water availability for vegetation. At even lower elevations below the bottom of the cloud layer decreasing rainfall amounts contribute to lower water availability again, although not as extreme as exists well above the inversion layer.

More work needs to be done in order to determine more quantitatively the importance of these summertime soil water deficits for plant communities along this transect and the animals that depend on them. Clearly, however, the extreme climates at the upper elevations must have served as significant environmental forces for the development of unique adaptations by Hawaiian plants and animals, many of which are found nowhere else in the world. If global warming does bring the relatively mesic climates found at 1650 and 2130 meters significantly upslope, then these plants and animals which are currently so well adapted may find themselves losing the competition with aggressive nonnative species.

DIURNAL CYCLE

Average diurnal patterns for each measurement are shown in Figures 37 through 45 and Table 4. Global radiation patterns reflect the greater attenuation of sunlight through the atmosphere and clouds at lower elevations (Figure 38). The pattern at 3000 meters is quite symmetrical, reflecting the generally cloud-free conditions at this elevation. The average daily solar radiation peak at this elevation occurs between 1200 and 1300 hours, halfway between average sunrise at 0700 hours and sunset at 1900 hours. At lower elevations global radiation peaks at progressively earlier hours on average, reflecting the influence of clouds earlier in the day. Global radiation peaks occur at 1200, 1200, 1100 and 1100 hours respectively at 2600, 2130, 1650 and 950 meters elevation. Afternoon global radiation is noticeably attenuated at 950 and 1650 meters. The greatest afternoon cloudiness occurs at the 1650 meter station in the cloud belt.

Near dusk (1800 to 1900 hours) precipitation increased dramatically to a peak of 15-17 mm/hr, probably as a result of rapidly lowering air temperatures with accompanying lower saturation vapor pressures. From midnight through 1400 hours on January 15 the freezing rain and snow continued at a lesser rate of 1-6 mm/hr. Relative humidity declined dramatically on the evening of January 15 as the inversion layer reformed below 3000 meters elevation. This inversion layer persisted through January 18.

Figure 47 shows air temperatures at 2600 and 3000 meters elevation, as well as ground temperature at 3000 meters. The ground temperature at 3000 meters began to drop sharply when precipitation began and hovered near zero from the night of January 14 through the day of January 15. With snow on the ground and clear skies on the night of January 15, ground temperature decreased dramatically to below -9 °C. From January 16 through 18 ground temperatures slowly returned to more normal levels as the snow melted. Air temperatures also decreased during the storm, but not as dramatically as ground temperatures. From this graph it is evident that events such as this storm can bring unusually low soil temperatures to high elevations on Haleakala, which may in turn act as an effective environmental constraint against species which cannot tolerate such low temperatures even for a night.

Figure 48 shows radiation patterns during the snowstorm. Of particular interest is the pattern of net radiation at 2600 and 3000 meters during the night of January 14. Apparently, freezing rain and snow during the night served to equalize soil and sky temperatures, and net radiation remained close to zero throughout the night. Before and after the storm net radiation maintained its more familiar pattern of negative nighttime values as the relatively warmer soil radiated energy into the atmosphere and space. Net radiation was higher at 3000 meters than at 2600 meters on January 13, as is typical. Through January 16, however, daytime net radiation at the summit was lower than at 2600 meters, probably as a result of the much greater albedo of the snow-covered ground at 3000 meters.

As this discussion indicates, extreme climate events such as this snowstorm can create environmental conditions well outside of the range normally found at a location. Such conditions, although infrequent, may play an important part in effecting changes in the distribution of plants and animals on the landscape. The climate stations in Haleakala National Park offer the opportunity to study these climate events in spatial and temporal detail, with the additional possibility of relating these events to the biology of affected plants and animals.

POTENTIAL EVAPORATION

The concept of potential evaporation (PE) has been developed as a way to describe the climatic influences on evaporation from a plant and the surrounding soil, and it is an important characteristic of plant water relations. PE can be defined as the evaporation from a short green vegetated surface for which water is not limiting. Penman (1948) developed an equation to estimate PE in given climatic conditions:

$$\lambda E = (\Delta R_N + \gamma E_A)/(\Delta + \gamma)$$

where λE is the latent heat flux of evaporating water
Δ is the slope of the saturation vapor pressure versus temperature curve
R_N is net radiation
γ is the psychrometric constant
and E_A is an aerodynamic term

Penman developed an empirical equation to estimate the aerodynamic term:

$$E_A = (0.013 + 0.00016U_2)(e^*_2 - e_2)$$

where U_2 is wind speed in km/day measured 2 meters above the ground
e^*_2 is saturation vapor pressure at air temperature 2 meters above the ground, and
e_2 is vapor pressure at air temperature 2 meters above the ground

Other researchers have used the basic Penman formulation with some modifications to estimate PE. Van Bavel developed a more physically based formulation for the aerodynamic term (Van Bavel 1966):

$$E_A = 3.64U_R(e^*_R - e_R)/T_R[\ln(z_R/z_0)]^2$$

where U_R is wind speed in km/day at the reference height
e^*_R is saturation vapor pressure at the reference height
e_R is vapor pressure at reference height
T_R is air temperature at reference height in degrees Kelvin

z_R is reference height, and
z_0 is the roughness length, a characteristic parameter of the surface

Priestly and Taylor (1972) developed a simplification of the Penman equation for use over large areas:

$$\lambda E = 1.26\Delta R_N/(\Delta + \gamma)$$

In the Priestly-Taylor formulation, then, the aerodynamic term is replaced by a constant. With these three formulations, PE was estimated for the five climate station sites using measurements of net radiation, air temperature, relative humidity and wind speed. For hours in which all of these instruments recorded error free data, and during which the atmometer also recorded error free data, direct comparisons could be made between these estimates and the atmometer measurements. Figures 49 through 53 show diurnal patterns comparing these paired atmometer measurements and PE estimates over the whole period of climate station operation.

Figure 49 shows this comparison for the station at 950 meters. This station has the closest fit of the 5 stations between atmometer and modeled PE values. However, the atmometer values seem to contain a time lag during the day that might be a result of inertia within the atmometer system. This time lag is evidenced by the atmometer values which are lower than modeled PE values in the morning hours and higher than modeled PE values during the afternoon. At midday, the atmometer peaks on average at 1300 hours while the PE estimates peak on average at 1200 hours.

Although this time lag could be the result of inertia within the atmometer system, the atmometer values could still be representing a more accurate estimate of environmental evaporation since it makes sense that there would be inertia in evaporation rates from the soil and plants as well. The other notable characteristic of Figure 49 is the nighttime evaporation, which is distinctly higher for the atmometer than for the PE estimates. In fact, all of the PE estimates predict negative nighttime evaporation, which can be interpreted as the condensation of dew.

In Figure 50, the atmometer evaporation at 1650 meters is reasonably well reproduced during the daytime with about a one hour lag time here also. The nighttime discrepancy between atmometer measurements and PE estimates is even greater here, however, with atmometer rates averaging about 2 mm/day higher.

In Figures 51 through 53, the upper stations have large discrepancies between atmometer measurements and PE estimates during both day and night. During the peak hours of the day, the atmometer rates of evaporation are from 3 to 6 mm/day lower than the PE rates estimated from the various Penman equations. During the night, this situation is reversed with the atmometer rates averaging from 1.5 to 3 mm/day higher than the PE estimates. One possible explanation for this phenomenon is the existence of large amounts of heat advection between the surface and the air which is not incorporated into the PE models (Nullet and Giambelluca 1990, Giambelluca and Nullet 1992). The atmometer values are consistent with the presence of relatively moist upslope winds during the daytime which would tend to suppress evaporation, while relatively dry downslope winds would tend to enhance evaporation. The PE models used in this analysis all have an assumption of equilibrium boundary layer conditions between the evaporating surface and the reference point where measurements are made. These equilibrium conditions are probably rarely met because of adiabatic changes in air temperature and relative humidity with the upslope and downslope winds. Further research on this issue is needed in order to better understand and predict potential evaporation rates.

DISCUSSION

Because of the persistent subsidence inversion at about 2000 meters elevation, a unique climate is created at high altitudes in the Hawaiian Islands, which in turn has led to unique adaptations by native plants. This report has documented a four year period of intensive climate monitoring for a high altitude leeward transect on East Maui. The information in this report may be useful for ecological monitoring in Haleakala National Park.

Several areas of potential research have been outlined. These climate stations serve as a continuing database for research into climate variability and the interaction between climate and ecological processes on leeward East Maui. In particular, this database serves as an excellent source of information for research on the relations between climate, native biota, and the deleterious

impacts of exotic biota on native ecosystems. Further research needs to be done to assess the impact of extreme climatic events and possible climate changes related to global warming on Hawaiian ecosystem dynamics, and these stations provide an excellent source of data for this research.

In addition to these climate stations, a series of four remotely-accessed climate stations have been installed on the windward side of East Maui within Haleakala National Park. These stations should provide similar data for the windward side of East Maui as the current stations are providing for the leeward side. The range of ecosystems monitored with detailed climate information will expand to include the Kalapawili grasslands as well as the O'hia forest and bogs below down to 1600 meters elevation within Haleakala National Park. These stations will provide unprecedented opportunities to study relationships between climate and ecological processes in these Hawaiian ecosystems.

It is hoped that this report will serve to stimulate further ecological research incorporating climatic events and processes in Hawaii, with an aim to developing successful research and management strategies for preserving these native Hawaiian ecosystems.

ACNOWLEDGEMENTS: This report would not have been possible without the financial assistance of the Research Division of Haleakala National Park and the Research Corporation of the University of Hawaii. We would like to especially thank Lloyd Loope, Cliff Smith and Pamela Waiolena for providing the infrastructural support to keep this project running. Sabine Jessel, Chuck Chimera and Kathy Wakely provided the invaluable and necessary field support to keep these climate stations operating and produce the data for this report, while Ron Nagata is providing critical logistical support to keep all 9 climate stations operating into the future. Finally, special thanks to Mike Nullet and Phillip Thomas for providing critical support with the computer systems throughout the project.

BIBLIOGRAPHY

Bird, R. E., Riordan, C. (1986). Simple solar spectral model for direct and diffuse irradiance on horizontal and tilted planes at the earth's surface for cloudless atmospheres. Journal of Climate and Applied Meteorology. 25:87-97.

Giambelluca, T. W., McKenna, D. L., Ekern, P. C. (1992). An automated recording atmometer: 1. calibration and testing. Journal of Agricultural and Forest Meteorology. 62:109-125.

Giambelluca, T. W., Nullet, D. (1992). Evaporation at high elevations in Hawaii. Journal of Hydrology. 136:219-235.

Lavoie, R. L. (1974). A numerical model of trade wind weather on Oahu. Monthly Weather Review. 102:630-637.

Nullet, D., Giambelluca, T. W. (1990). Winter evaporation on a mountain slope, Hawaii. Journal of Hydrology. 112:257-265.

Penman, H. L. (1948). Natural evaporation from open water, soil and grass. Proceedings of the Royal Society of London, Series A. 193:120-145.

Priestley, C. H. B., Taylor, R. J. (1972). On the assessment of surface heat flux and evaporation using large-scale parameters. Monthly Weather Review. 100(2):81-92.

Riehl, H., Yeh, T. C., Malkus, J. J., La Seur, N. E. (1951). The northeast trade of the Pacific Ocean. Quarterly Journal of the Royal Meteorological Society. 77:598-626.

Selling, O. H. (1948). Studies in Hawaiian pollen statistics. Part III. On the late Quaternary history of the Hawaiian vegetation. Bernice P. Bishop Museum Special Publication 39.

Van Bavel, C. H. M. (1966). Potential evapotranspiration: the combination concept and its experimental verification. Water Resources Research. 2:455-467.

Table 1: Monthly Averages of Climate Measurements Along Climate Transect

Net Radiation (W/m^2)

	elevation (m)				
	950	1650	2130	2600	3000
Jun-88	142.6	118.0	174.2		
Jul-88	144.6	116.2	158.6		
Aug-88	125.4	95.1	148.5		
Sep-88	116.4	96.3	130.7		
Oct-88	97.4	85.2	107.1		
Nov-88	85.6	71.1	95.7		
Dec-88	74.9	63.3	94.0		
Jan-89	91.0	68.2	103.2		
Feb-89	90.4	76.8	109.6		
Mar-89	115.8	99.0	145.5		
Apr-89	130.4	103.1	134.8		
May-89	132.5	108.6	162.5		
Jun-89	128.4	115.1	156.7		
Jul-89	120.4	109.0	179.1		
Aug-89	111.0	105.8	161.1		
Sep-89	106.0	93.6	142.5		
Oct-89		86.4	127.9		
Nov-89	78.2	88.9	102.7		
Dec-89	63.6	80.5	85.0		
Jan-90	61.6	66.9	91.7		
Feb-90	86.8	79.5	103.5		
Mar-90	105.1	88.9	141.2	138.2	
Apr-90	106.5	88.2	131.1	136.0	175.6
May-90	127.9	108.8	152.9	161.1	188.7
Jun-90	110.6	105.9	165.7	179.2	201.3
Jul-90	108.5	101.6	144.9	154.4	186.0
Aug-90	119.2	108.4	162.9	161.7	195.1
Sep-90	101.7	88.6	129.6	140.7	179.6
Oct-90	95.9	83.6	112.8	118.8	154.2
Nov-90	65.0	63.1	89.6	81.9	102.5
Dec-90	69.1	69.8	92.3	77.3	100.3
Jan-91	88.6	69.2	108.9	82.0	121.7
Feb-91	93.4	84.8	118.3	117.6	141.6
Mar-91	92.9	82.2	117.9	123.7	151.4
Apr-91	117.7	88.7	138.9	146.8	215.2
May-91	121.8	96.7	137.1	143.5	202.1
Jun-91	129.9	96.4	127.2	153.4	211.1
Jul-91	116.2	92.3	134.5	152.2	215.0
Aug-91	118.2	97.3	142.4	147.4	197.8
Sep-91	104.0	89.4	131.8	141.2	199.5
Oct-91	86.2	73.4	112.1	110.4	168.7
Nov-91	79.1	67.4	98.3	86.2	144.2
Dec-91	67.6	62.1	93.8	79.2	113.7
Jan-92	83.1	78.1	107.8	92.1	118.4
Feb-92	104.3	98.8	132.6	123.6	151.6
Mar-92	107.8	96.8	148.4	136.0	179.0
Apr-92	123.5	92.6			

Global Radiation (W/m^2)

	elevation (m)				
	950	1650	2130	2600	3000
Jun-88	221.0	209.3	328.5		
Jul-88	232.8	197.2	280.8		
Aug-88	204.2		245.8		
Sep-88	190.8	162.1	205.6		
Oct-88	163.2	152.1	170.6		
Nov-88	148.7	138.9	159.0		
Dec-88	136.9	126.2	151.5		
Jan-89	158.2	128.8	192.2		
Feb-89	148.6	135.0			
Mar-89	183.0	165.8	232.5		
Apr-89	199.1	167.1	187.5		
May-89	212.4	174.3	243.9		
Jun-89	210.4	182.5	265.2		
Jul-89	204.2	172.8	266.2		
Aug-89	194.9	172.3	238.5		
Sep-89	188.8	156.2	202.5		
Oct-89		132.8	159.6		
Nov-89	153.7	149.4	153.7		
Dec-89	138.2	138.1			
Jan-90	128.3	131.4			
Feb-90	158.8	151.7			
Mar-90	186.6	170.3	267.3	312.8	
Apr-90	181.9	153.8	226.1	265.8	303.7
May-90	228.7	183.6	255.0	301.1	325.8
Jun-90	215.7	182.5	288.3	314.3	325.3
Jul-90	209.9	174.9	248.5	279.0	296.5
Aug-90	226.8	185.0	266.2	303.7	318.5
Sep-90	191.3	151.7	200.1	248.6	262.3
Oct-90	183.8	146.2	176.1	215.6	235.6
Nov-90	114.9	109.2	132.2	152.5	145.9
Dec-90	139.4	130.2	154.2	157.1	153.7
Jan-91	172.2	164.3	195.4	210.0	214.4
Feb-91	189.2	176.8	208.0	219.2	223.6
Mar-91	176.6	162.9	192.6	208.9	212.6
Apr-91	217.6	168.0	241.9	294.1	322.1
May-91	224.8	178.6	251.4	290.5	317.8
Jun-91	226.7	177.0	257.7	268.3	328.5
Jul-91	212.1	166.6	246.1	287.8	322.3
Aug-91	207.8	175.9	241.6	223.6	279.3
Sep-91	188.9	161.7	216.6	230.0	273.1
Oct-91	161.1	141.0	189.9	212.2	236.8
Nov-91	151.3	132.7	181.1	202.8	205.0
Dec-91	141.4	124.3	161.9	176.1	191.3
Jan-92	154.0	156.1	206.7		213.9
Feb-92	187.0	185.8	236.1	213.2	246.4
Mar-92	199.7	171.3	248.3	216.9	304.0
Apr-92	224.2	170.8			

Table 1 continued

	Air Temperature (°C)					Relative Humidity (%)				
	elevation (m)					elevation (m)				
	950	1650	2130	2600	3000	950	1650	2130	2600	3000
Jun-88	18.0	15.9	14.8			77.0				
Jul-88	18.2	15.7	12.5			76.6		62.8		
Aug-88	18.4	15.2	12.2			79.9		69.3		
Sep-88	18.8	15.7	12.8			80.4		66.2		
Oct-88		15.2	11.6					71.3		
Nov-88		15.3	11.1					69.5		
Dec-88			9.5					71.7		
Jan-89			8.5					73.4		
Feb-89										
Mar-89										
Apr-89										
May-89										
Jun-89										
Jul-89										
Aug-89										
Sep-89			11.8					71.8		
Oct-89		15.1	13.3				83.7	73.3		
Nov-89	17.6	13.6	12.8			80.4	74.3	54.7		
Dec-89	15.9	11.6	10.1			80.8	72.9	60.4		
Jan-90	16.4	13.0				86.0	74.2	48.0		
Feb-90	15.0	10.9	8.7			84.0	79.8	71.5		
Mar-90	15.7	11.4	11.1	11.3		83.2	78.3	52.3	23.1	
Apr-90	17.1	12.8	12.5	11.1	10.2	85.6	81.5	59.0	46.8	31.9
May-90	17.5	13.0	11.7	11.0		81.6	81.2	66.6	47.7	33.0
Jun-90	18.6	14.4	14.1	13.3	10.5	84.0	81.3	57.9	36.7	33.9
Jul-90	19.0	15.0	13.6	11.9	9.3	85.3	81.2	67.7	60.3	50.2
Aug-90	19.7	15.3	14.1	13.2	10.8	83.2	81.0	65.8	51.2	40.1
Sep-90	19.8	15.3	13.5	12.1	9.5	84.6	85.9	79.2	69.5	63.3
Oct-90	19.0	14.6	12.3	11.2	9.1	82.9	81.0	75.9	63.2	51.9
Nov-90	18.4	14.6	13.0	11.0	8.3	91.2	86.8	80.2	76.8	73.9
Dec-90	16.5	12.6	10.8	8.6	6.0	83.9	74.7	65.5	59.2	54.6
Jan-91	15.5	12.2	11.4	10.1	7.8	58.0	65.8	45.5	32.2	26.2
Feb-91	16.2	12.5	11.0	9.5	6.9	83.4	70.7	60.8	51.3	46.3
Mar-91	15.6	11.6	9.5	7.6	4.7	86.8	82.4	77.0	69.1	68.2
Apr-91	16.8	12.1	11.2	10.2	7.9	85.5	85.6	63.7	48.0	39.6
May-91	17.5	12.7	11.8	10.8	8.6	84.8	83.9	66.3	49.3	38.3
Jun-91	18.1	13.3	11.8	11.0	9.3	84.5	85.5	72.2	53.1	38.0
Jul-91	19.1	14.5	13.7	13.1	11.1	86.3	86.7	66.7	47.4	37.2
Aug-91	19.9	15.7	14.5	12.5	10.3	87.2	84.4	71.8	63.0	57.2
Sep-91	19.3	14.9	14.0	14.9	9.6	87.8	85.6	68.9	59.3	55.2
Oct-91	18.8	14.2	13.2		9.8	86.4	86.7	70.8	55.1	47.6
Nov-91	18.6	14.4	14.1		9.8	85.1	79.9	56.1	41.6	38.9
Dec-91	16.6	12.5	11.8	11.0	7.9	86.6	78.6	58.3	44.9	39.0
Jan-92	15.2	11.6	11.3	10.2	8.2	82.5	69.5	42.7	25.0	22.3
Feb-92	15.2	11.5	11.5	9.0	6.1	83.6	65.3	45.4	35.4	38.8
Mar-92	15.8	10.8	10.8	10.3	8.1	83.7	83.7	52.6	27.7	21.1
Apr-92	16.4	11.3				77.7	76.3			

Table 1 continued

	Vapor Pressure (mb)					Wind Speed (m/s)				
	elevation (m)					elevation (m)				
	950	1650	2130	2600	3000	950	1650	2130	2600	3000
Jun-88	15.8					0.2	1.7	3.3		
Jul-88	15.8		8.9			0.9	2.0	3.0		
Aug-88	16.9		10.0			0.8	1.8	2.3		
Sep-88	17.2		10.4			0.8	1.9	2.4		
Oct-88			9.7			0.5	2.1	2.3		
Nov-88			9.1			0.2	2.4	1.8		
Dec-88			8.5			0.6	2.5	2.7		
Jan-89			8.1			0.6	3.2	3.3		
Feb-89										
Mar-89										
Apr-89										
May-89										
Jun-89										
Jul-89										
Aug-89										
Sep-89			10.3					1.0		
Oct-89		14.5	11.2				1.5	1.6		
Nov-89	16.3	11.8	8.1			1.1	2.0	2.0		
Dec-89	14.8	10.2	7.6			1.4	2.4	2.0		
Jan-90	16.1	11.2				1.0	2.1	3.5		
Feb-90	14.4	10.6	8.0			1.3	2.8	2.6		
Mar-90	14.9	10.7	6.8	3.1		1.2	2.2	2.5	1.8	
Apr-90	16.8	12.2	8.3	5.9	3.0	1.0	1.5	2.2	2.4	4.1
May-90	16.4	12.4	9.1	6.1		1.2	1.7	2.2	2.1	4.3
Jun-90	17.9	13.5	9.0	5.2	4.0	1.1	1.5	3.3	3.1	6.0
Jul-90	18.8	14.0	10.5	8.4	5.8	1.1	1.7	2.2	2.2	4.3
Aug-90	19.2	14.4	10.8	7.8	5.2	1.2	1.7	2.2	2.1	3.4
Sep-90	19.5	15.1	12.4	9.8	7.4	1.1	1.6	2.2	2.2	3.8
Oct-90	18.6	13.8	11.2	8.5	5.9	1.1	1.8	1.9	1.8	3.3
Nov-90	19.4	14.6	12.1	10.0	8.1	1.0	2.0	2.4	3.4	4.0
Dec-90	15.8	11.0	8.5	6.5	4.9	1.5	3.4	3.6	4.2	4.8
Jan-91	10.3	9.3	6.0	3.9	1.9	1.6	3.2	3.2	3.6	3.9
Feb-91	15.5	10.4	8.0	5.9	4.4	1.6	2.9	3.1	3.7	4.0
Mar-91	15.6	11.5	9.2	7.1	5.7	1.2	3.3	4.1	3.2	5.0
Apr-91	16.4	12.3	8.5	5.9	4.1	1.2	1.8	1.9	2.4	4.1
May-91	16.9	12.6	9.2	6.2	4.1	1.2	1.9	2.3	2.4	4.1
Jun-91	17.6	13.3	10.1	7.0	4.5	1.3	2.0	1.9	2.0	3.5
Jul-91	19.1	14.4	10.4	7.0	4.8	1.1	1.8	1.7	2.2	4.4
Aug-91	20.3	15.2	11.9	9.0	7.0	1.1	2.4	2.4	2.2	4.2
Sep-91	19.6	14.7	10.9	9.0	6.5	1.1	1.8	1.9	2.5	4.1
Oct-91	18.7	14.3	10.8		5.6	1.1	1.8	1.2	2.1	3.5
Nov-91	18.4	13.3	9.0		4.7	1.0	1.9	1.8	3.0	4.9
Dec-91	16.5	11.7	8.1	5.6	4.1	1.0	2.2	2.6	2.5	4.0
Jan-92	14.3	9.5	5.6	3.0	2.3	1.4	2.5	1.6		3.7
Feb-92	14.8	9.0	6.2	4.2	3.6	2.1	3.6	3.3	6.3	4.5
Mar-92	15.1	11.0	6.8	3.4	2.2	1.1	2.0	2.0	2.2	3.7
Apr-92	14.6	10.5				1.1	2.1			

Table 1 continued

	Rainfall (mm/day)					Atmometer Evaporation (mm/day)				
	elevation (m)					elevation (m)				
	950	1650	2130	2600	3000	950	1650	2130	2600	3000
Jun-88							1.6	7.0		
Jul-88						3.3	4.4	6.3		
Aug-88						3.7	3.1			
Sep-88							3.4	3.5		
Oct-88						1.6	3.2	2.5		
Nov-88						2.4	3.6	3.0		
Dec-88						2.3	2.8			
Jan-89							3.4	1.8		
Feb-89										
Mar-89										
Apr-89										
May-89										
Jun-89										
Jul-89										
Aug-89						3.6	3.0	4.0		
Sep-89		0.0	0.8				4.5	2.8		
Oct-89		4.3	4.5					2.5		
Nov-89	1.2	0.7	0.7			2.5				
Dec-89	5.9	5.7	5.5					3.4		
Jan-90	3.9	8.1	14.8					4.8		
Feb-90	4.3	0.0	7.8			2.8	4.3	3.4		
Mar-90	1.1	0.1	4.4			4.0	3.3	6.4	9.0	
Apr-90	0.3	0.9	0.7	0.4	0.5	3.1	2.4	5.3	9.0	9.6
May-90	0.4	0.8	3.1	1.3	0.3			3.6	5.8	
Jun-90	0.2	0.8	3.1	1.5	0.7	3.3	3.8	5.9	4.9	8.3
Jul-90	0.5	0.8	2.8	1.0	1.2		5.6	4.9	4.1	6.2
Aug-90	0.1	0.1	1.0	0.5	0.3			5.0	5.5	8.1
Sep-90	0.5	1.5	4.7	2.4	1.6	4.5		3.6	3.2	
Oct-90	0.6	1.4	2.2	3.3	2.9	3.8	2.9	2.9	4.0	5.2
Nov-90	7.3	8.7	15.7	18.7	24.5	2.5	2.2	2.3	3.8	2.9
Dec-90	4.3	4.8	7.6	10.1	12.9	2.3	4.0	2.6	3.5	5.1
Jan-91	1.6	3.6	4.0	4.5	9.0	3.0	4.0	3.6	5.2	6.5
Feb-91	1.2	2.8	5.5	3.2	3.0	4.0	4.2	2.6	4.4	4.7
Mar-91	3.2	8.6	23.6	18.9	12.5	3.2	3.6	1.4	3.4	5.0
Apr-91	0.2	0.6	0.6	0.7	0.7	4.0	3.1	3.6	6.0	6.1
May-91	0.4	0.8	0.7	0.3	0.2	4.5	3.3	4.7	6.3	7.3
Jun-91	0.6	0.7	1.3	0.3	0.1	4.8	3.3	3.9	5.8	7.3
Jul-91	0.1	1.4	1.1	0.9	0.5	4.4	3.8	4.0	7.3	7.7
Aug-91	0.9	4.1	7.6	5.9	3.0	4.3	4.0	3.2	5.3	5.1
Sep-91		6.3	3.4	1.9	2.4	3.9	3.7	2.6	5.8	5.2
Oct-91		1.1	0.5	0.8	0.7	4.5	3.0	2.0	4.4	3.1
Nov-91	0.8	6.3	3.4	1.9	2.4	3.9	3.7	2.6	5.8	5.3
Dec-91	0.4	1.1	1.0	0.8	1.1	3.2	2.8	1.8	3.7	4.3
Jan-92	0.3	0.2	0.5	0.3	0.4	3.5	3.9	1.9	4.7	6.2
Feb-92	0.9	1.0	2.6	1.8	1.2	2.8	4.1	1.5	3.2	5.3
Mar-92	3.4	5.0	4.7	4.1	2.0	3.4	5.9	1.8	3.4	6.2
Apr-92	1.5	1.1	0.6	0.5	2.7	5.1	8.6	1.6	4.0	5.4
	0.0	0.1	0.1	0.1	0.1	3.8	3.3	2.6	4.4	6.2
		0.0				5.0	3.6			

Table 1 continued

Soil Heat Flux (W/m^2)

	elevation (m)				
	950	1650	2130	2600	3000
Mar-90	-1.1	-1.0	0.7		
Apr-90	0.1	0.4	-0.1		
May-90	0.9	0.3	0.4		
Jun-90	2.2	0.2	0.6		
Jul-90	0.7	0.0	-0.3		
Aug-90	2.9	0.0	-0.6		
Sep-90	1.1	-0.6	-0.4	-2.9	-2.0
Oct-90	0.4	-1.6	-1.3	-1.9	-3.2
Nov-90	-0.3	-0.1	0.3	-1.0	-3.3
Dec-90	-2.9	-1.5	-2.1	-1.5	-5.2
Jan-91	-2.4	-0.7	-1.4	3.1	-1.0
Feb-91	-1.8	0.1	0.4	1.2	-2.0
Mar-91	0.5	0.2	1.5	1.2	-0.7
Apr-91	2.9	0.8	2.2	0.6	2.6
May-91	1.0	1.5	1.0	0.8	4.7
Jun-91	2.0	1.1	0.7	0.2	5.8
Jul-91	2.1	1.8	0.6	-0.2	3.3
Aug-91	-0.2	2.3	1.4	-0.1	0.0
Sep-91	-1.8	0.0	-0.3	-3.7	-2.5
Oct-91	-0.8	0.0	-0.3	1.1	-2.4
Nov-91	-1.6	-0.2	-0.8	5.4	-2.3
Dec-91	-2.0	-1.0	-1.3	2.1	-4.6
Jan-92	-1.6	-0.2	-1.0		-2.7
Feb-92	-0.9	-0.2	0.7	-5.2	-3.1
Mar-92	-0.1	0.0	0.5	-6.1	1.5
Apr-92	1.6	-0.1			

Table 2: Elevational Patterns of Climate Along Climate Transect

		elevation (m)				
		950	1650	2130	2600	3000
annual mean values	net radiation (W/m^2)	103.4	89.5	128.5	127.1	167.9
	global radiation (W/m^2)	184.7	159.4	216.7	242.2	260.8
	modelled clear sky (W/m^2)	294.8	301.4	304.0	305.3	306.5
	cloud attenuation (%)	37.4	47.1	28.7	20.7	14.9
	net/global radiation (%)	56.0	56.1	59.3	52.5	64.4
	air tempurature (^oC)	17.6	13.5	12.1	11.0	8.7
	relative humidity (%)	83.3	80.4	64.1	50.3	43.5
	wind speed (m/s)	1.1	2.1	2.4	2.8	4.1
	soil heat flux (W/m^2)	0.0	0.0	0.0	0.0	0.0
	rainfall (mm/year)	462.0	896.7	1525.1	1215.1	1276.0
	rainfall (mm/day)	1.3	2.5	4.2	3.3	3.5
	atmometer evaporation (mm/day)	3.7	3.6	3.4	5.0	6.1
	vapor pressure (mb)	16.9	12.6	9.1	6.8	4.8
June and July mean values	net radiation (W/m^2)	123.9	106.1	153.7	159.7	203.3
	global radiation (W/m^2)	216.4	179.7	269.3	287.4	318.0
	modelled clear sky (W/m^2)	348.0	355.6	358.6	360.0	361.5
	cloud attenuation (%)	37.8	49.5	24.9	20.2	12.0
	net/global radiation (%)	57.3	59.1	57.1	55.6	63.9
	air tempurature (^oC)	18.5	14.6	13.3	12.3	10.0
	relative humidity (%)	82.7	83.7	65.5	50.0	39.9
	wind speed (m/s)	1.0	1.8	2.5	2.3	4.6
	soil heat flux (W/m^2)	1.7	0.6	0.4	0.0	4.5
	rainfall (mm/day)	0.4	0.9	2.1	0.9	0.6
	atmometer evaporation (mm/day)	4.2	3.9	4.7	5.9	7.3
	vapor pressure (mb)	17.6	13.8	9.8	7.0	4.8
December and January mean values	net radiation (W/m^2)	74.9	69.5	97.5	82.5	112.9
	global radiation (W/m^2)	146.1	137.1	177.3	187.0	193.3
	modelled clear sky (W/m^2)	218.7	223.9	226.0	227.0	228.0
	cloud attenuation (%)	33.2	38.8	21.5	17.6	15.2
	net/global radiation (%)	51.3	50.7	55.0	44.1	58.4
	air tempurature (^oC)	16.0	12.3	10.8	9.8	7.5
	relative humidity (%)	79.3	72.7	55.8	40.7	35.5
	wind speed (m/s)	1.2	2.7	2.7	3.5	4.1
	soil heat flux (W/m^2)	-2.2	-0.9	-1.5	1.7	-3.3
	rainfall (mm/day)	3.3	4.7	6.3	5.3	6.3
	atmometer evaporation (mm/day)	2.9	3.8	2.6	4.0	5.8
	vapor pressure (mb)	14.6	10.5	7.2	4.8	3.4

Table 3: Annual Climate Pattern Along Climate Transect

Net Radiation (W/m^2)

	elevation (m)				
	950	1650	2130	2600	3000
Jan	81.1	70.6	103.7	86.8	120.3
Feb	93.8	83.9	115.6	120.6	146.6
Mar	105.3	91.7	137.5	131.8	166.0
Apr	118.6	93.3	135.1	141.4	202.5
May	127.4	104.7	150.8	152.2	195.4
Jun	125.3	107.6	153.2	166.3	206.2
Jul	122.5	104.8	154.2	153.3	200.5
Aug	118.5	101.7	153.8	154.5	196.5
Sep	107.2	91.9	133.5	140.9	189.6
Oct	93.2	82.1	115.3	114.6	161.4
Nov	78.4	72.9	96.7	84.0	123.3
Dec	68.8	68.5	91.3	78.2	105.5

Global Radiation (W/m^2)

	elevation (m)				
	950	1650	2130	2600	3000
Jan	153.2	144.7	199.6	208.3	214.1
Feb	170.9	160.5	222.0	217.2	235.0
Mar	186.5	165.6	231.9	239.0	259.6
Apr	200.9	163.1	219.0	280.0	315.7
May	221.9	178.8	250.1	295.8	321.8
Jun	218.1	184.8	278.4	291.5	326.9
Jul	214.7	174.7	260.4	283.4	309.4
Aug	208.4	177.8	248.1	292.7	298.9
Sep	190.0	157.9	206.3	239.3	267.7
Oct	169.4	143.0	174.4	213.9	236.2
Nov	141.9	132.5	155.9	177.6	170.9
Dec	139.0	129.5	155.0	165.8	172.5

Air Temperature (^oC)

	elevation (m)				
	950	1650	2130	2600	3000
Jan	15.7	12.3	11.0	10.2	8.1
Feb	15.5	11.7	10.5	9.3	6.6
Mar	15.7	11.3	10.5	9.5	6.6
Apr	16.9	12.4	11.8	10.7	8.3
May	17.5	12.8	11.7	10.9	8.7
Jun	18.3	14.3	13.3	12.1	9.9
Jul	18.8	15.0	13.2	12.5	10.2
Aug	19.3	15.4	13.7	12.8	10.5
Sep	19.5	15.3	13.4	12.6	9.5
Oct	18.9	14.8	12.7	11.2	9.5
Nov	18.2	14.4	13.2	11.0	9.0
Dec	16.3	12.3	10.6	9.4	6.9

Relative Humidity (%)

	elevation (m)				
	950	1650	2130	2600	3000
Jan	74.9	69.9	47.5	28.7	24.3
Feb	83.7	72.6	58.9	43.3	42.6
Mar	84.6	81.5	61.1	42.4	41.9
Apr	84.9	82.8	61.4	47.4	37.2
May	83.2	82.6	66.5	48.5	35.7
Jun	82.8	83.4	65.0	47.0	35.9
Jul	82.7	84.0	66.0	52.8	43.7
Aug	83.4	82.7	69.0	57.2	48.7
Sep	85.6	85.7	72.0	64.4	59.2
Oct	84.8	84.0	72.9	59.2	49.7
Nov	85.4	80.5	64.3	59.2	56.4
Dec	83.8	75.5	64.0	52.8	46.8

Vapor Pressure (mb)

	elevation (m)				
	950	1650	2130	2600	3000
Jan	13.5	10.0	6.2	3.4	2.2
Feb	14.9	10.1	7.4	5.0	4.0
Mar	15.2	11.1	7.7	4.7	3.8
Apr	16.4	12.1	8.4	5.9	3.9
May	16.7	12.5	9.1	6.2	4.1
Jun	17.4	13.4	9.6	6.3	4.2
Jul	17.9	14.2	10.0	7.6	5.3
Aug	18.8	14.8	10.9	8.4	6.1
Sep	19.4	14.9	11.3	9.7	7.0

Windspeed (m/s)

	elevation (m)				
	950	1650	2130	2600	3000
Jan	1.3	2.7	2.8	3.6	3.8
Feb	1.7	3.1	3.0	4.7	4.2
Mar	1.2	2.5	2.9	2.5	4.1
Apr	1.1	1.7	2.1	2.4	4.1
May	1.2	1.8	2.3	2.3	4.2
Jun	1.0	1.8	2.7	2.5	4.8
Jul	1.0	1.8	2.3	2.2	4.4
Aug	1.1	2.0	2.3	2.1	3.8
Sep	1.0	1.8	2.1	2.3	3.9

Table 3 continued

Oct	18.7	14.2	10.8	8.5	5.8	1.0	1.8	1.7	2.0	3.4
Nov	18.0	13.3	9.7	10.0	6.4	0.9	2.0	2.1	3.2	4.4
Dec	15.7	11.0	8.2	6.2	4.5	1.1	2.6	2.7	3.4	4.4

Rainfall (mm/day)

	elevation (m)					Atmometer Evaporation (mm/day) elevation (m)				
	950	1650	2130	2600	3000	950	1650	2130	2600	3000
Jan	3.0	5.6	7.4	4.3	5.5	3.3	4.1	3.0	4.7	6.3
Feb	2.3	2.1	4.6	1.9	2.9	4.4	4.7	2.4	4.3	5.0
Mar	1.5	3.2	10.0	7.2	6.3	3.6	3.4	3.6	4.9	5.5
Apr	0.2	0.7	0.6	0.6	0.6	3.9	3.0	4.3	6.4	7.2
May	0.4	0.8	1.9	0.8	0.2	4.5	3.3	4.6	6.3	7.7
Jun	0.4	0.8	2.2	0.9	0.4	4.5	3.4	4.7	5.6	7.6
Jul	0.3	1.1	2.0	1.0	0.9	4.0	4.3	4.7	6.1	7.1
Aug	0.5	2.1	4.3	3.2	1.6	4.0	3.5	3.8	5.3	6.7
Sep	0.6	3.8	3.5	2.2	2.0	4.2	3.8	3.0	4.9	5.3
Oct	0.5	2.3	2.6	2.0	2.0	3.3	3.0	2.4	3.9	4.8
Nov	4.2	3.2	5.8	9.5	12.5	2.8	3.5	2.2	4.3	4.3
Dec	3.7	3.8	5.2	6.3	7.1	2.5	3.5	2.2	3.4	5.2

Soil Heat Flux (W/m^2)

	elevation (m)				
	950	1650	2130	2600	3000
Jan	-2.0	-0.5	-1.2	3.3	-1.6
Feb	-1.3	0.0	0.5	-0.9	-2.5
Mar	-0.1	-0.2	0.9	-2.4	0.4
Apr	1.5	0.5	1.1	0.6	2.6
May	0.9	0.8	0.7	0.8	4.7
Jun	2.1	0.4	0.6	0.2	5.8
Jul	1.4	0.8	0.1	-0.2	3.3
Aug	1.4	0.6	0.4	-0.1	0.0
Sep	-0.3	-0.3	-0.4	-3.2	-2.2
Oct	-0.2	-0.8	-0.8	-0.4	-2.8
Nov	-1.0	-0.2	-0.3	2.2	-2.8
Dec	-2.4	-1.2	-1.7	0.1	-5.0

Table 4: Diurnal Climate Pattern Along Climate Transect

Net Radiation (W/m^2)

	elevation (m)				
	950	1650	2130	2600	3000
1:00 AM	-22.3	-27.9	-35.4	-62.6	-55.2
2:00 AM	-23.1	-28.4	-35.2	-61.7	-54.3
3:00 AM	-24.0	-28.7	-35.0	-60.9	-53.4
4:00 AM	-24.5	-29.1	-34.6	-60.4	-52.7
5:00 AM	-24.9	-29.4	-34.4	-60.2	-52.3
6:00 AM	-25.2	-29.8	-34.1	-59.9	-51.8
7:00 AM	-14.2	-15.4	-23.8	-49.2	-27.0
8:00 AM	64.2	74.9	59.6	73.3	99.7
9:00 AM	220.6	236.9	237.5	263.0	300.1
10:00 AM	338.5	351.0	399.1	440.2	476.0
11:00 AM	376.7	370.9	493.6	537.4	597.3
12:00 PM	373.8	331.6	516.9	570.6	664.5
1:00 PM	349.2	294.3	490.6	560.0	669.8
2:00 PM	323.3	259.4	440.3	506.8	636.9
3:00 PM	283.2	221.1	372.5	425.6	550.1
4:00 PM	219.8	171.7	281.9	310.2	412.3
5:00 PM	139.3	107.5	171.9	165.2	251.8
6:00 PM	54.4	41.6	54.7	14.8	70.0
7:00 PM	-5.2	-6.2	-22.3	-68.8	-48.7
8:00 PM	-19.4	-19.1	-36.5	-72.0	-67.7
9:00 PM	-18.8	-21.5	-36.3	-68.2	-63.2
10:00 PM	-19.5	-24.4	-36.1	-66.2	-60.4
11:00 PM	-20.1	-25.9	-36.0	-64.4	-58.0
12:00 AM	-21.2	-27.0	-35.5	-63.3	-56.2

Global Radiation (W/m^2)

	elevation (m)				
	950	1650	2130	2600	3000
1:00 AM	0.0	0.1	0.1	0.1	0.4
2:00 AM	0.0	0.1	0.1	0.1	0.4
3:00 AM	0.0	0.1	0.1	0.1	0.4
4:00 AM	0.0	0.3	0.1	0.1	0.4
5:00 AM	0.0	0.4	0.1	0.1	0.4
6:00 AM	0.3	0.4	0.4	0.3	0.9
7:00 AM	18.2	26.6	22.6	11.3	33.9
8:00 AM	126.2	170.5	155.0	87.8	183.1
9:00 AM	344.9	383.2	371.9	342.7	403.7
10:00 AM	524.3	518.5	569.2	590.9	598.6
11:00 AM	576.9	541.0	684.9	727.9	741.3
12:00 PM	570.6	483.1	712.5	787.5	820.4
1:00 PM	532.6	428.3	679.4	781.9	840.1
2:00 PM	497.3	380.8	614.7	727.1	796.4
3:00 PM	445.9	330.1	526.3	646.8	698.1
4:00 PM	370.3	266.1	414.6	526.9	549.4
5:00 PM	262.1	185.3	285.7	364.1	376.9
6:00 PM	132.1	91.5	135.5	176.0	172.3
7:00 PM	29.1	18.2	27.0	36.0	38.6
8:00 PM	0.3	0.2	0.4	0.3	1.4
9:00 PM	0.1	0.1	0.1	0.1	0.5
10:00 PM	0.1	0.1	0.1	0.9	0.5
11:00 PM	0.0	0.1	0.1	0.4	0.5
12:00 AM	0.0	0.1	0.1	0.1	0.4

Air Temperature (^oC)

	elevation (m)				
	950	1650	2130	2600	3000
1:00 AM	15.3	11.4	10.2	9.2	6.8
2:00 AM	15.1	11.3	10.1	9.1	6.8
3:00 AM	14.9	11.2	10.0	9.0	6.7
4:00 AM	14.8	11.1	9.9	8.9	6.6
5:00 AM	14.7	11.0	9.8	8.8	6.6
6:00 AM	14.6	11.0	9.8	8.8	6.6
7:00 AM	14.8	11.4	10.1	8.9	6.9
8:00 AM	16.4	13.4	11.7	10.0	8.0
9:00 AM	18.4	15.4	13.3	11.6	9.3
10:00 AM	19.7	16.2	14.3	12.9	10.3
11:00 AM	20.4	16.4	14.9	13.6	11.0
12:00 PM	20.7	16.3	15.0	14.0	11.4
1:00 PM	20.9	16.2	15.0	14.1	11.6
2:00 PM	21.0	16.1	14.9	14.0	11.6
3:00 PM	21.0	15.9	14.8	13.8	11.5

Relative Humidity (%)

	elevation (m)				
	950	1650	2130	2600	3000
1:00 AM	88.0	75.8	58.9	46.6	42.5
2:00 AM	87.1	74.7	58.3	46.7	42.7
3:00 AM	86.3	73.7	58.4	47.2	43.0
4:00 AM	85.4	72.9	58.7	47.7	42.9
5:00 AM	84.6	71.7	58.5	47.5	42.7
6:00 AM	83.7	70.5	58.2	46.7	42.4
7:00 AM	82.5	69.3	57.4	46.2	41.8
8:00 AM	79.2	66.9	56.0	45.3	41.2
9:00 AM	76.4	68.7	56.6	45.2	40.7
10:00 AM	75.7	75.3	60.9	47.1	41.7
11:00 AM	75.5	81.7	66.3	50.6	43.3
12:00 PM	75.6	85.6	70.7	54.6	45.2
1:00 PM	76.4	87.8	73.5	57.6	46.7
2:00 PM	76.9	89.4	75.5	59.8	48.1
3:00 PM	77.4	90.4	75.7	60.3	48.5

Table 4 continued

4:00 PM	20.7	15.7	14.5	13.5	11.1	78.7	90.8	75.0	59.6	48.1
5:00 PM	20.2	15.4	14.1	13.0	10.5	81.1	91.5	73.8	57.3	46.5
6:00 PM	19.3	14.7	13.3	12.2	9.6	84.8	92.0	71.0	53.4	43.9
7:00 PM	18.0	13.6	12.0	10.8	8.5	89.3	91.2	67.9	51.0	42.3
8:00 PM	16.9	12.7	11.1	10.0	7.7	92.0	88.7	64.5	48.6	41.7
9:00 PM	16.4	12.3	10.8	9.8	7.4	91.8	85.0	62.2	47.1	41.6
10:00 PM	16.0	12.0	10.7	9.6	7.3	91.3	81.2	60.5	46.5	41.2
11:00 PM	15.7	11.7	10.6	9.5	7.1	90.3	79.1	59.7	46.6	41.7
12:00 AM	15.5	11.6	10.4	9.3	7.0	89.0	77.3	59.6	46.7	42.5

Vapor Pressure (mb)

	elevation (m)				
	950	1650	2130	2600	3000
1:00 AM	15.4	10.3	7.3	5.6	4.1
2:00 AM	15.1	10.0	7.1	5.6	4.1
3:00 AM	14.8	9.8	7.1	5.6	4.1
4:00 AM	14.5	9.7	7.1	5.7	4.1
5:00 AM	14.3	9.5	7.0	5.6	4.0
6:00 AM	14.1	9.4	7.0	5.5	4.0
7:00 AM	14.1	9.4	7.1	5.5	4.1
8:00 AM	14.9	10.4	7.6	5.7	4.3
9:00 AM	16.3	12.0	8.5	6.2	4.5
10:00 AM	17.4	13.9	9.8	7.0	5.0
11:00 AM	18.1	15.1	11.0	8.0	5.4
12:00 PM	18.5	15.8	11.9	8.8	5.8
1:00 PM	18.9	16.1	12.4	9.3	6.1
2:00 PM	19.1	16.2	12.6	9.6	6.3
3:00 PM	19.2	16.3	12.5	9.5	6.3
4:00 PM	19.2	16.1	12.1	9.2	6.1
5:00 PM	19.2	15.8	11.6	8.6	5.7
6:00 PM	19.0	15.3	10.6	7.6	5.1
7:00 PM	18.6	14.2	9.3	6.7	4.5
8:00 PM	17.9	13.0	8.4	6.1	4.3
9:00 PM	17.3	12.1	7.9	5.8	4.2
10:00 PM	16.8	11.4	7.7	5.7	4.1
11:00 PM	16.3	10.9	7.5	5.6	4.1
12:00 AM	15.8	10.6	7.4	5.6	4.2

Wind Speed (m/s)

	elevation (m)				
	950	1650	2130	2600	3000
1:00 AM	0.6	2.4	2.6	2.9	4.1
2:00 AM	0.6	2.4	2.6	2.9	4.1
3:00 AM	0.7	2.5	2.5	2.9	4.0
4:00 AM	0.7	2.5	2.5	2.9	4.0
5:00 AM	0.7	2.5	2.5	2.9	4.0
6:00 AM	0.7	2.6	2.5	2.9	4.0
7:00 AM	0.7	2.5	2.5	2.8	4.1
8:00 AM	0.5	1.8	2.2	2.7	4.1
9:00 AM	0.7	1.6	2.1	2.6	4.2
10:00 AM	1.2	1.8	2.3	2.6	4.2
11:00 AM	1.5	2.0	2.4	2.7	4.3
12:00 PM	1.8	2.1	2.4	2.8	4.3
1:00 PM	2.1	2.2	2.4	2.8	4.3
2:00 PM	2.3	2.2	2.4	2.8	4.2
3:00 PM	2.4	2.2	2.3	2.8	4.1
4:00 PM	2.3	2.1	2.2	2.7	4.1
5:00 PM	2.1	1.9	2.1	2.6	4.0
6:00 PM	1.7	1.5	2.0	2.5	4.0
7:00 PM	1.0	1.4	2.1	2.5	4.0
8:00 PM	0.5	1.7	2.4	2.6	4.0
9:00 PM	0.5	2.0	2.6	2.7	4.1
10:00 PM	0.5	2.2	2.7	2.8	4.2
11:00 PM	0.5	2.3	2.7	2.8	4.2
12:00 AM	0.5	2.4	2.6	2.9	4.2

Rainfall (mm/day)

	elevation (m)				
	950	1650	2130	2600	3000
1:00 AM	1.4	3.0	4.7	2.7	2.6
2:00 AM	0.6	1.4	3.8	3.1	2.5
3:00 AM	0.5	1.3	3.4	2.8	2.5
4:00 AM	0.7	1.1	3.5	2.9	2.5
5:00 AM	0.6	1.0	2.8	2.8	2.9
6:00 AM	0.8	0.8	2.8	2.4	2.1
7:00 AM	0.8	1.0	2.9	3.5	3.2

Atmometer Evaporation (mm/day)

	elevation (m)				
	950	1650	2130	2600	3000
1:00 AM	0.8	1.9	1.6	2.6	3.1
2:00 AM	0.9	2.0	1.6	2.5	3.0
3:00 AM	0.9	2.0	1.5	2.5	3.0
4:00 AM	0.9	2.1	1.5	2.5	3.0
5:00 AM	0.9	2.2	1.5	2.5	3.0
6:00 AM	0.9	2.3	1.5	2.6	3.1
7:00 AM	1.2	2.5	1.5	2.7	3.3

Table 4 continued

8:00 AM	0.6	1.4	3.4	3.1	3.1	2.0	2.9	1.9	3.4	4.2
9:00 AM	0.8	1.1	2.9	2.9	3.9	4.1	4.8	3.8	5.0	6.2
10:00 AM	0.6	1.4	3.4	3.7	4.1	7.3	7.3	6.1	7.3	9.0
11:00 AM	1.0	2.2	3.8	4.2	5.3	9.2	8.2	7.5	9.5	11.1
12:00 PM	1.4	3.0	4.6	4.5	6.1	9.7	7.7	7.9	10.5	12.4
1:00 PM	2.3	5.3	6.0	4.4	7.2	9.6	7.0	7.6	10.8	12.7
2:00 PM	2.2	6.2	6.7	4.8	5.8	9.3	6.3	7.0	10.2	12.3
3:00 PM	2.3	5.5	5.9	3.9	4.9	8.6	5.7	6.2	9.3	11.2
4:00 PM	1.9	6.7	5.7	3.2	3.6	7.6	4.9	5.0	8.1	9.6
5:00 PM	1.7	3.7	4.7	3.0	2.7	5.9	3.8	4.0	6.5	7.8
6:00 PM	2.4	3.0	5.0	3.7	3.2	3.9	2.6	3.0	4.9	6.1
7:00 PM	2.0	3.0	4.9	4.0	3.7	2.0	1.8	2.3	3.5	4.6
8:00 PM	1.0	2.0	4.4	3.2	2.1	1.0	1.7	1.8	2.8	3.7
9:00 PM	0.7	1.0	2.7	2.4	2.2	0.7	1.7	1.7	2.6	3.5
10:00 PM	0.9	1.0	3.5	2.9	2.6	0.7	1.8	1.7	2.6	3.4
11:00 PM	0.8	1.4	3.9	2.9	2.7	0.7	1.8	1.7	2.6	3.2
12:00 AM	0.6	1.7	4.9	3.1	2.4	0.8	1.9	1.6	2.6	3.1

Soil Heat Flux (W/m^2)

	elevation (m)				
	950	1650	2130	2600	3000
1:00 AM	-13.8	-8.4	-18.1	-16.4	-24.9
2:00 AM	-14.2	-8.6	-17.8	-16.3	-24.3
3:00 AM	-14.5	-8.7	-17.4	-16.0	-23.6
4:00 AM	-14.6	-8.7	-17.1	-15.8	-23.0
5:00 AM	-14.8	-8.8	-16.7	-15.6	-22.4
6:00 AM	-14.8	-8.8	-16.4	-15.4	-21.7
7:00 AM	-14.6	-8.6	-15.8	-15.0	-20.7
8:00 AM	-12.3	-7.6	-13.0	-13.8	-16.1
9:00 AM	-5.1	-4.7	-7.7	-10.5	-3.7
10:00 AM	9.8	0.4	-1.6	-2.1	14.4
11:00 AM	25.4	7.1	10.5	10.3	33.6
12:00 PM	32.1	12.8	22.9	22.2	48.9
1:00 PM	32.7	15.2	31.5	29.9	58.0
2:00 PM	30.9	15.1	36.9	34.1	60.1
3:00 PM	28.2	14.3	36.4	34.7	56.2
4:00 PM	23.4	12.2	31.5	32.1	46.8
5:00 PM	17.0	9.4	22.5	25.6	32.9
6:00 PM	9.1	5.8	9.7	14.2	15.6
7:00 PM	0.1	1.3	-6.0	1.3	-3.2
8:00 PM	-6.8	-2.8	-14.9	-9.5	-16.3
9:00 PM	-10.0	-5.4	-17.9	-14.5	-22.6
10:00 PM	-11.5	-6.8	-18.7	-16.2	-25.0
11:00 PM	-12.5	-7.7	-18.6	-16.7	-25.5
12:00 AM	-13.2	-8.1	-18.4	-16.6	-25.3

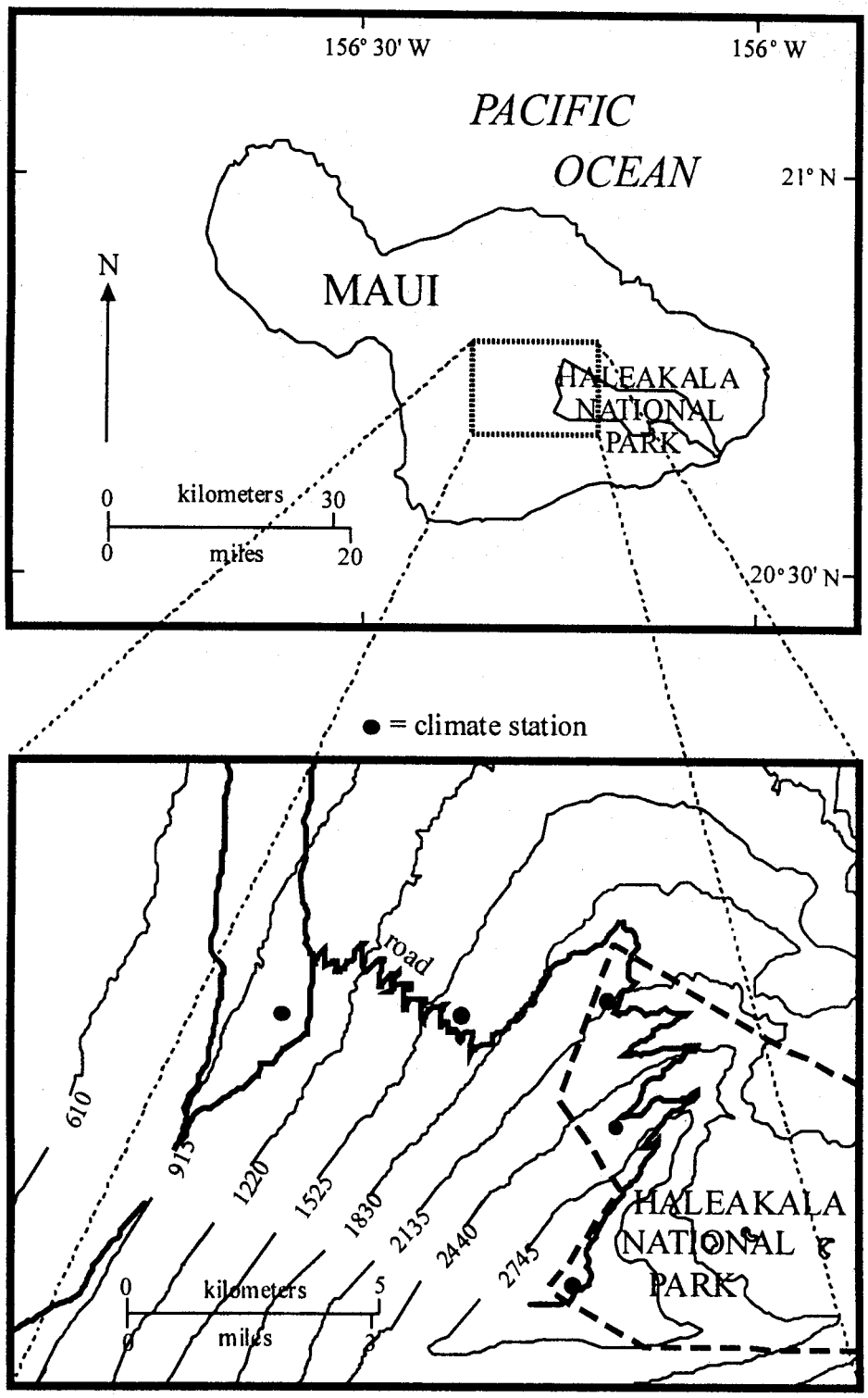

Figure 1 - Map of the Study Area. Contour interval is in meters.

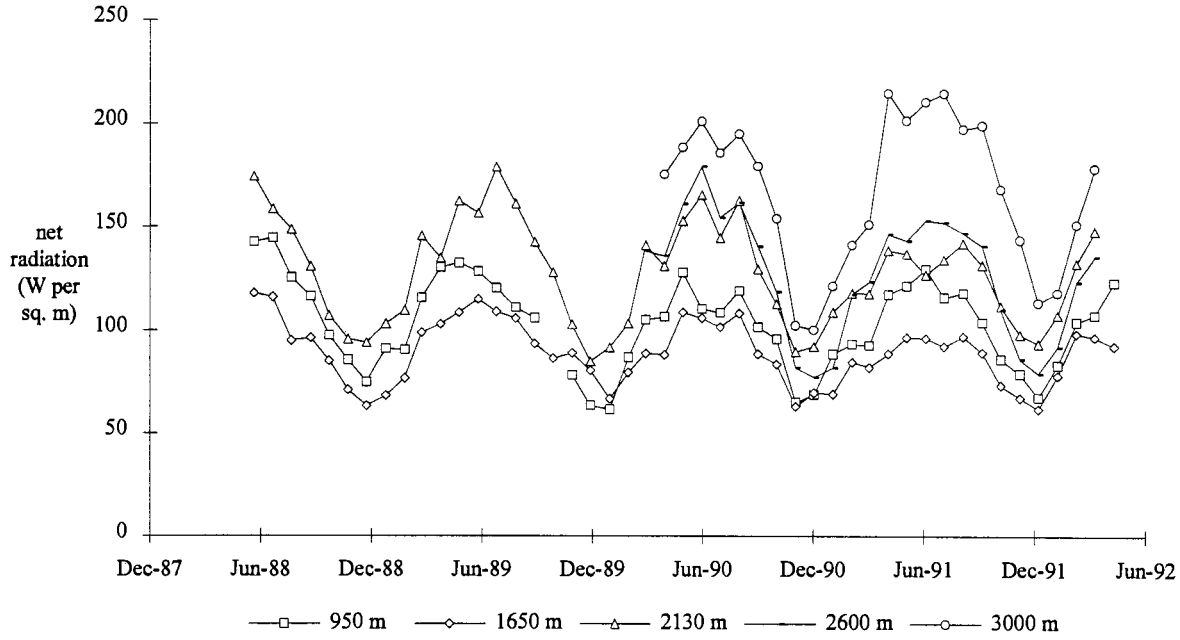

Figure 2 - Monthly Mean Net Radiation

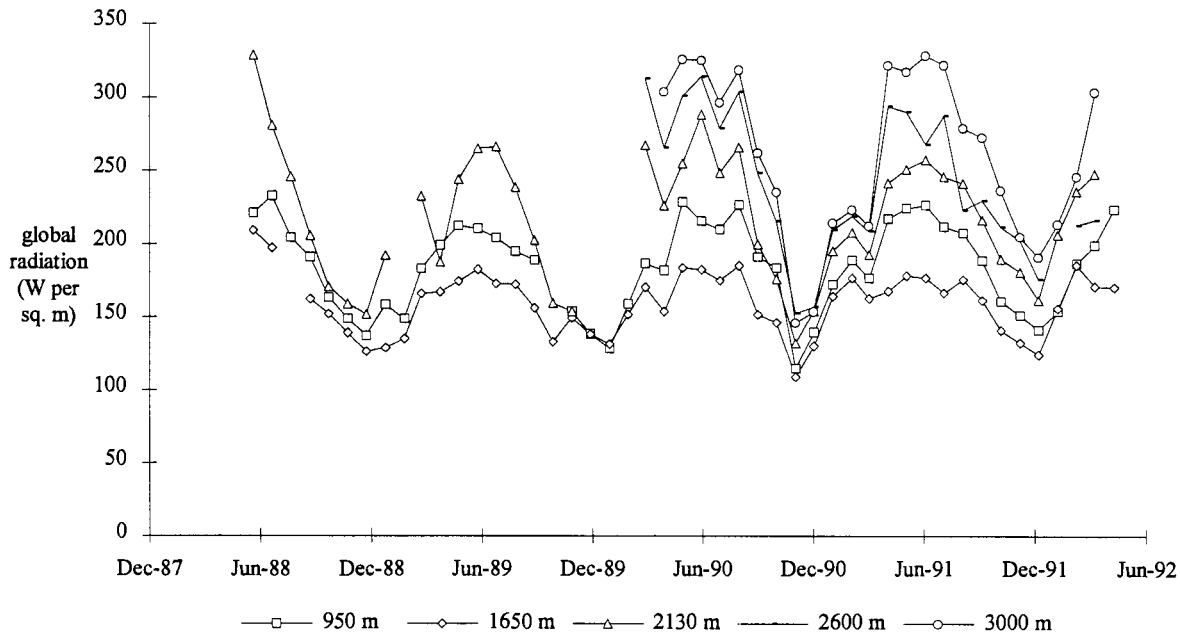

Figure 3 - Monthly Mean Global Radiation

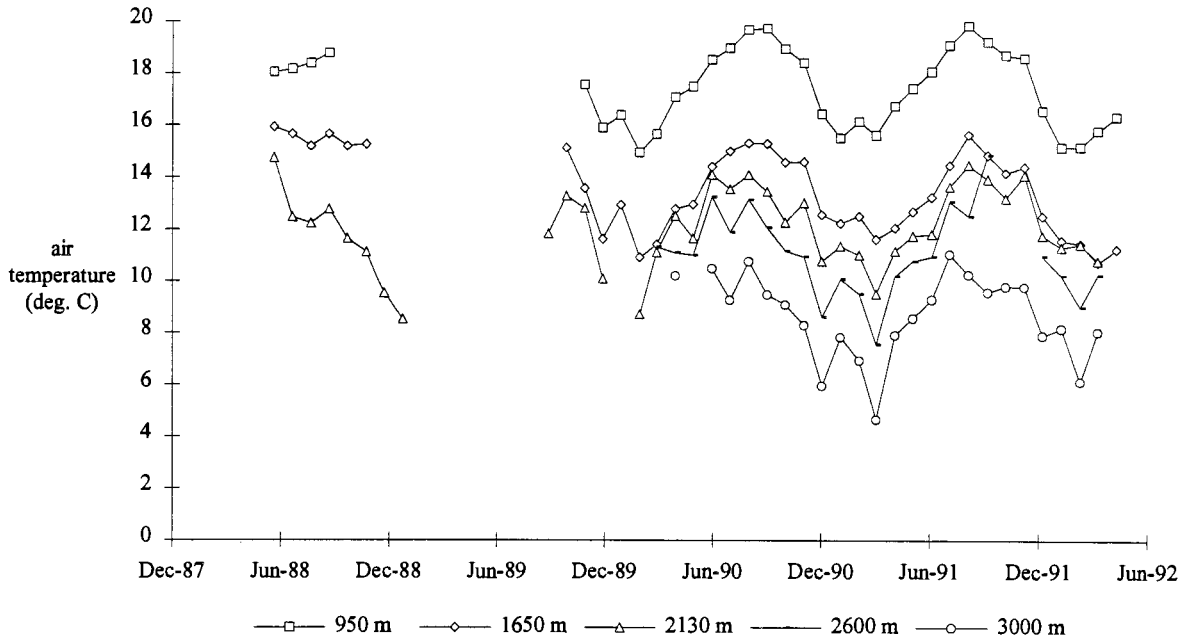

Figure 4 - Monthly Mean Air Temperature

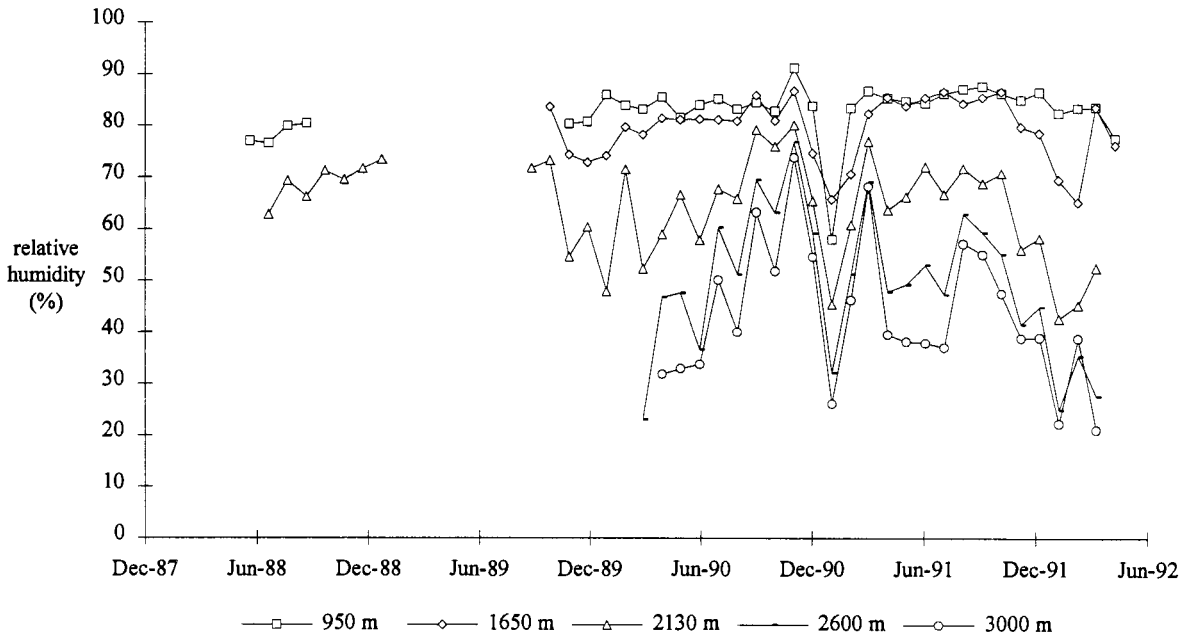

Figure 5 - Monthly Mean Relative Humidity

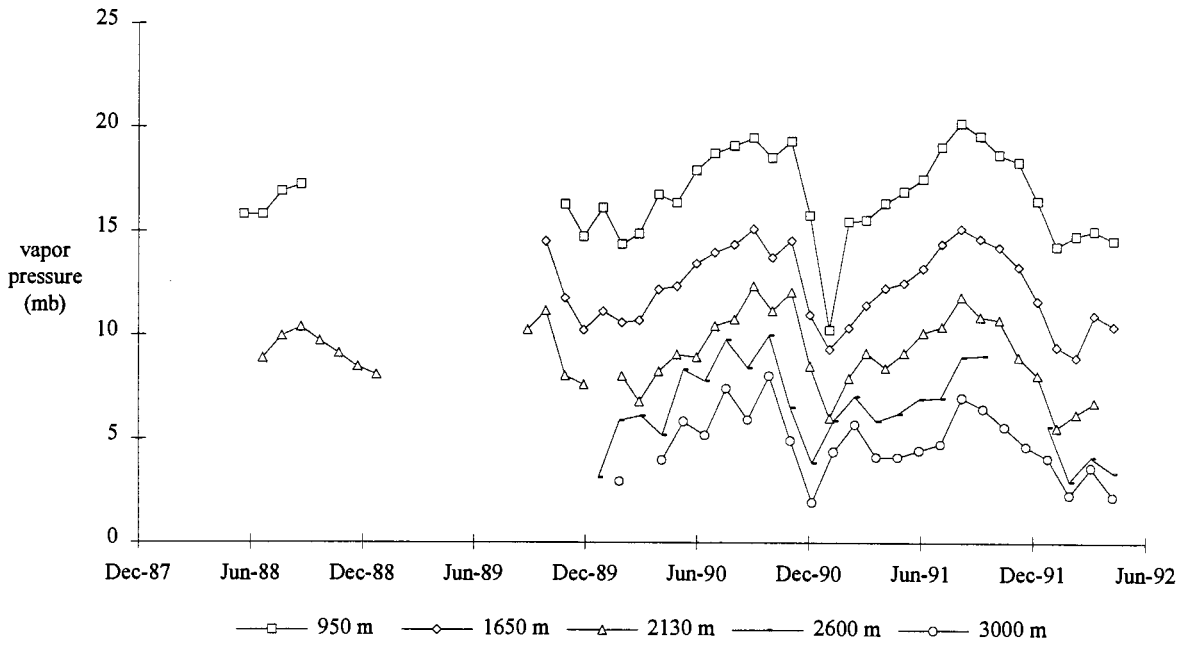

Figure 6 - Monthly Mean Vapor Pressure

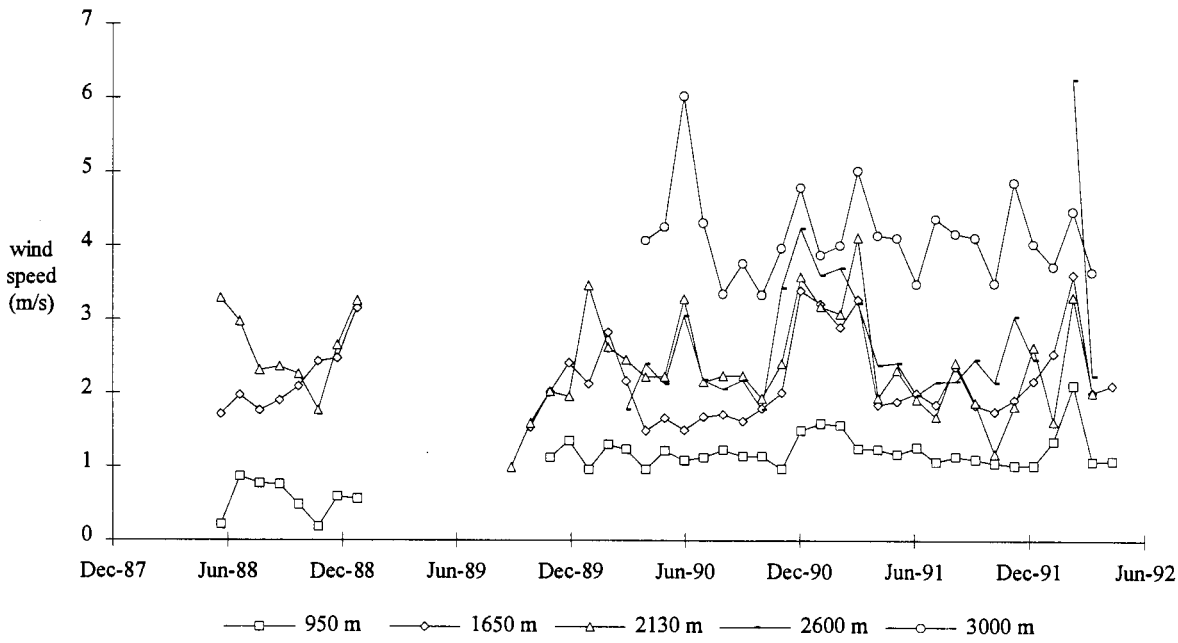

Figure 7 - Monthly Mean Wind Speed

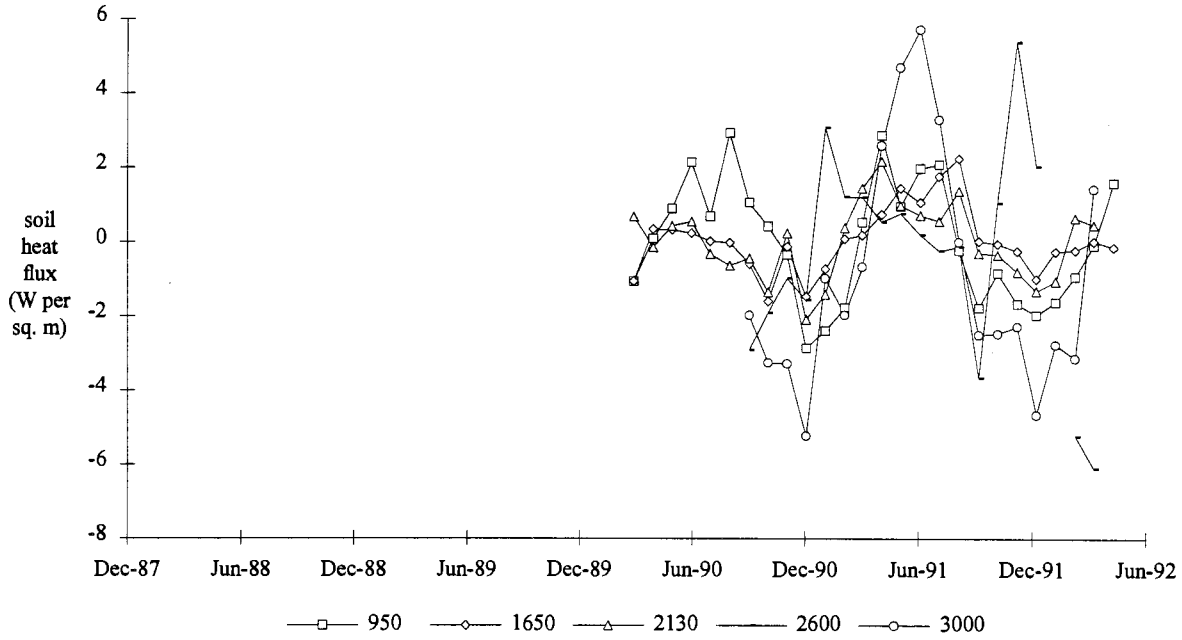

Figure 8 - Monthly Mean Soil Heat Flux

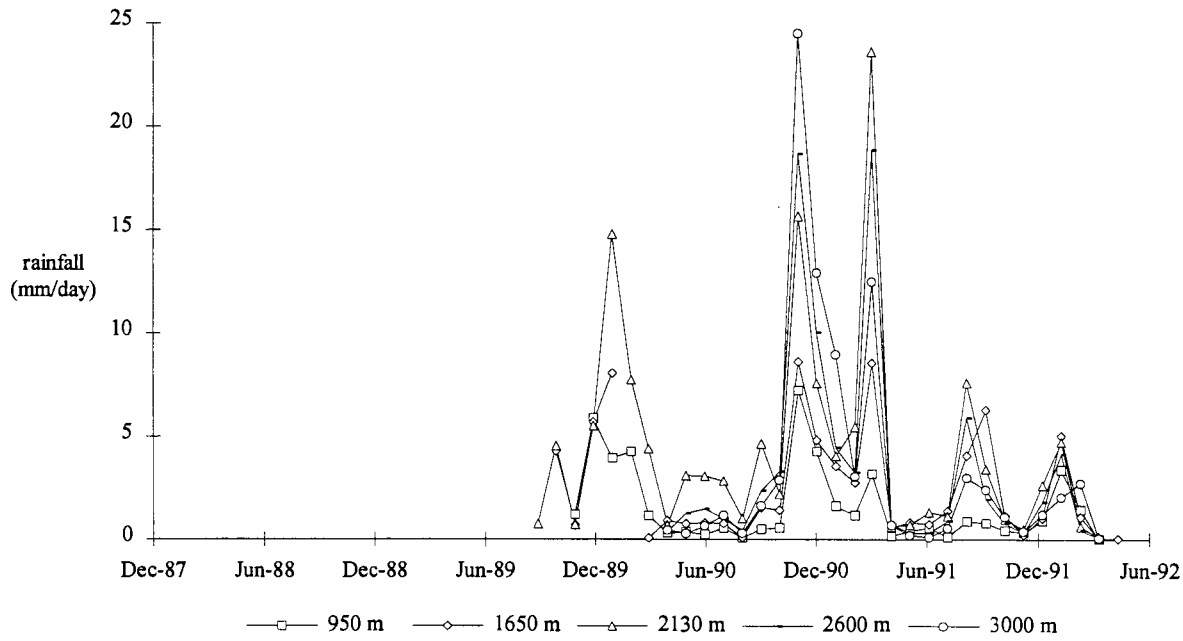

Figure 9 - Monthly Mean Rainfall

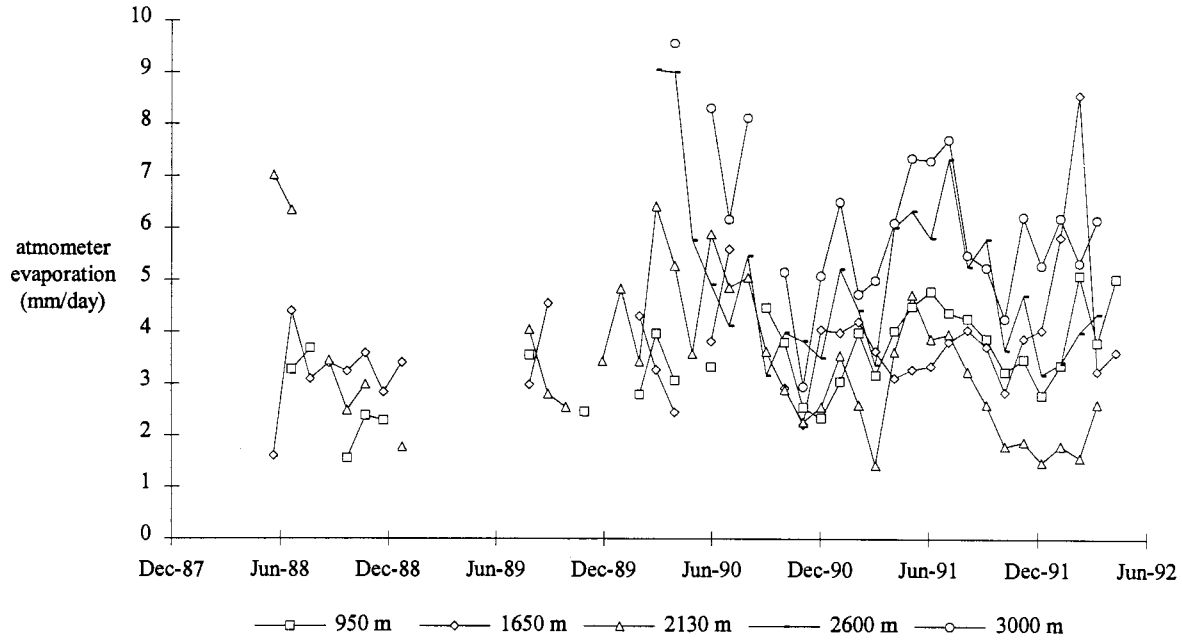

Figure 10 - Monthly Mean Atmometer Evaporation

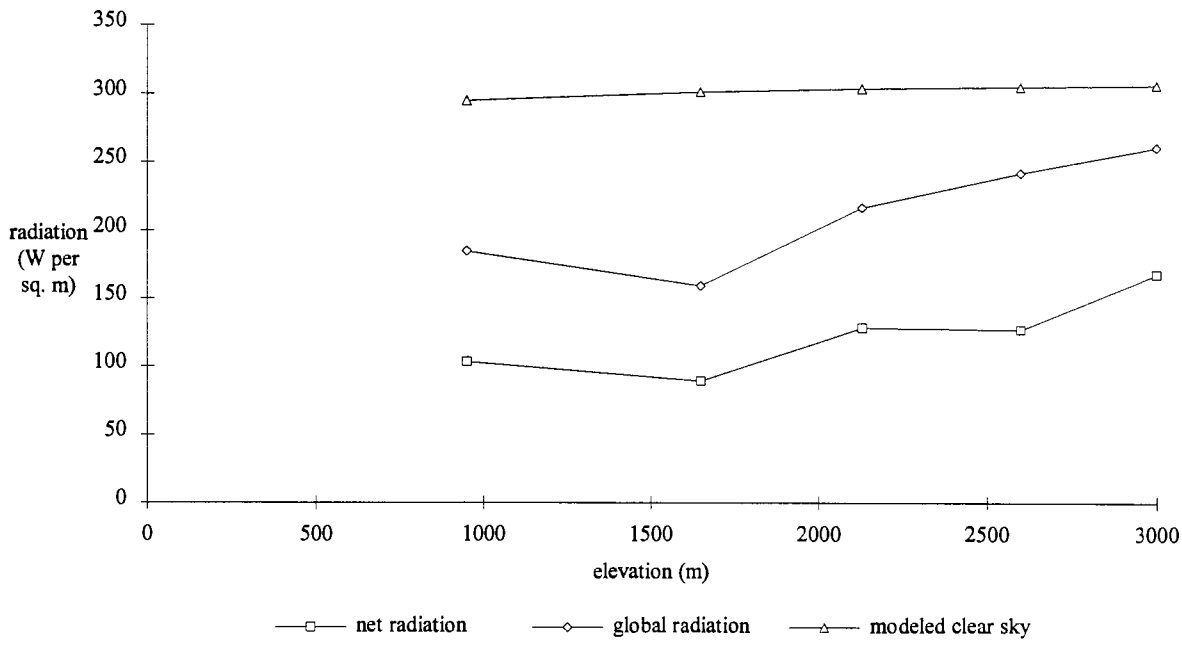

Figure 11 - Annual Mean Solar Radiation

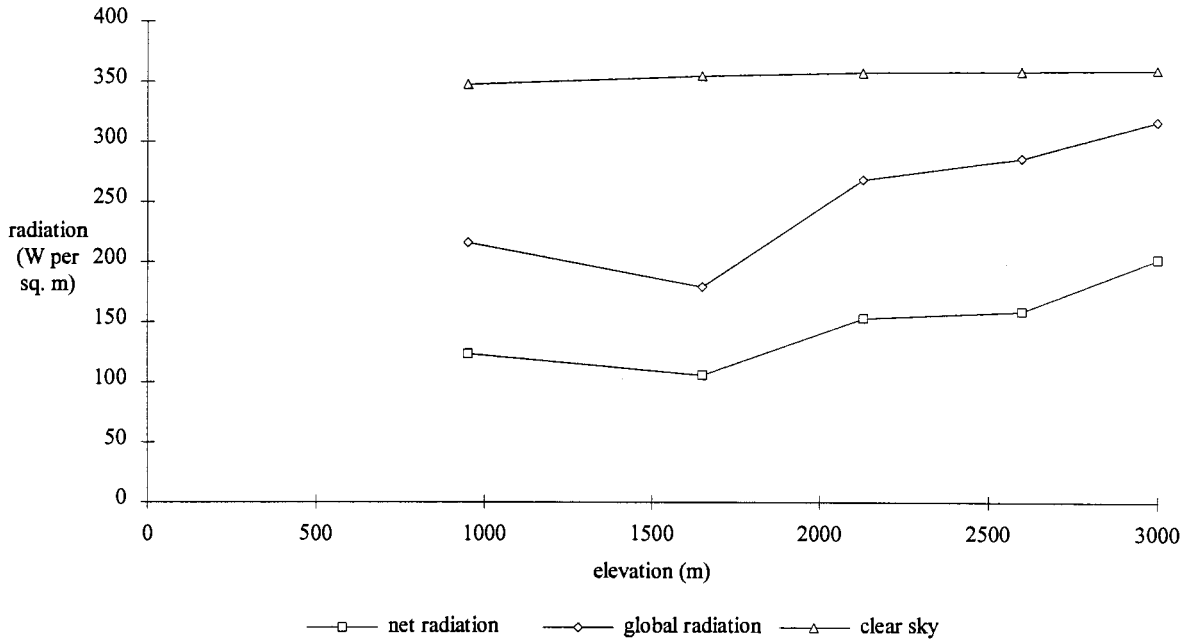

Figure 12 - June-July Mean Solar Radiation

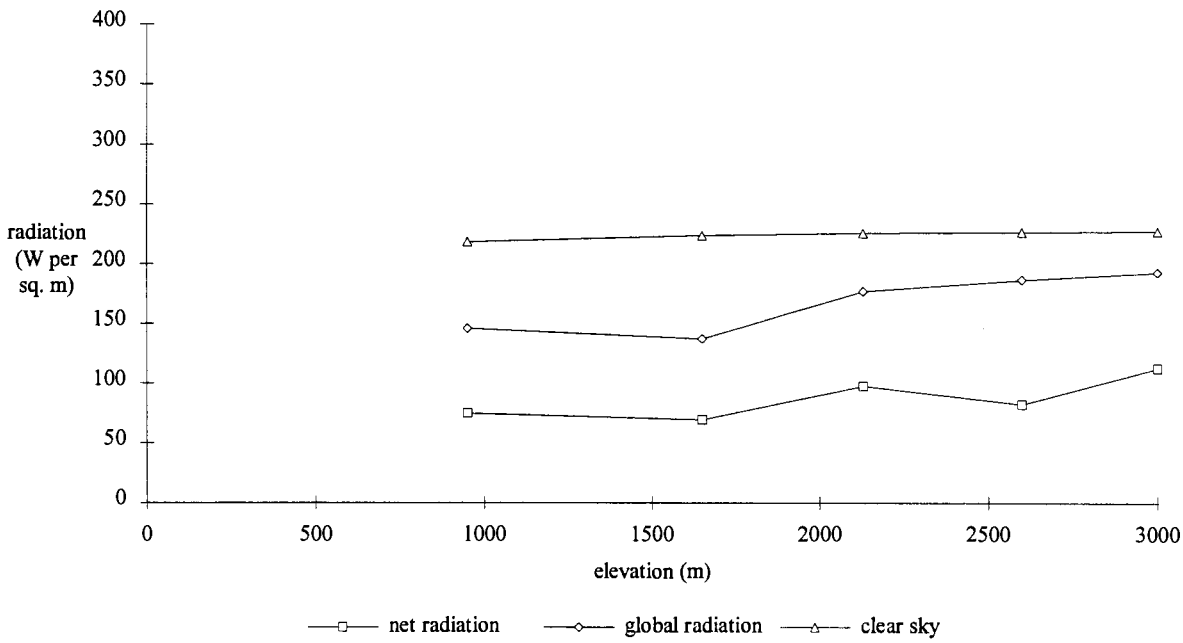

Figure 13 - December-January Mean Solar Radiation

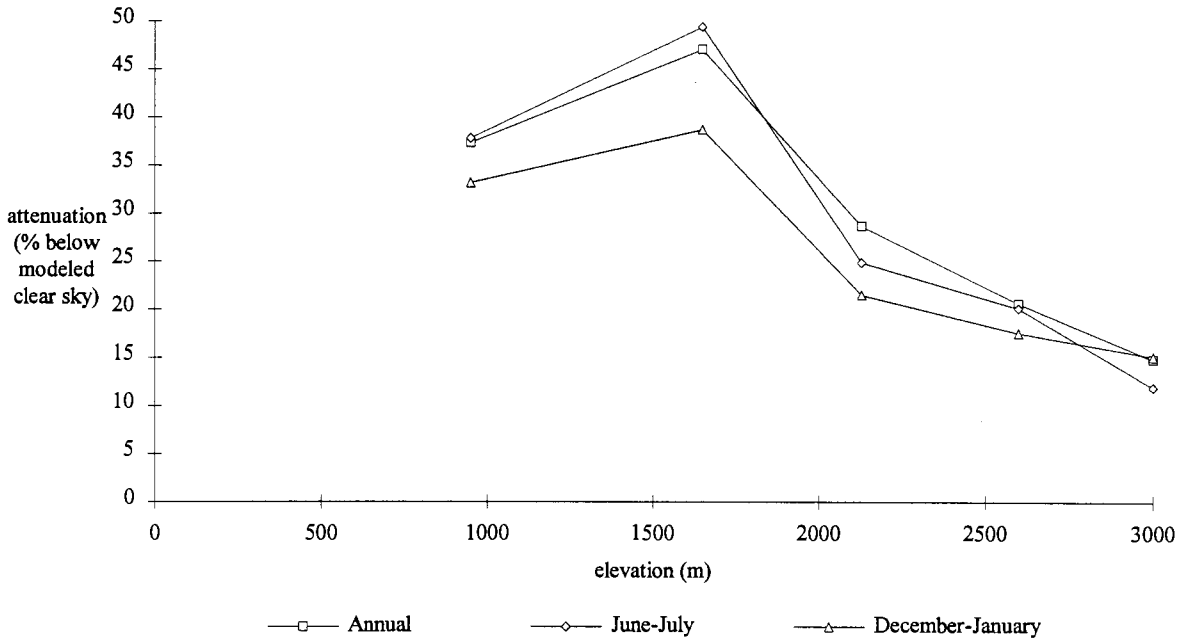

Figure 14 - Cloud Attenuation of Global Radiation

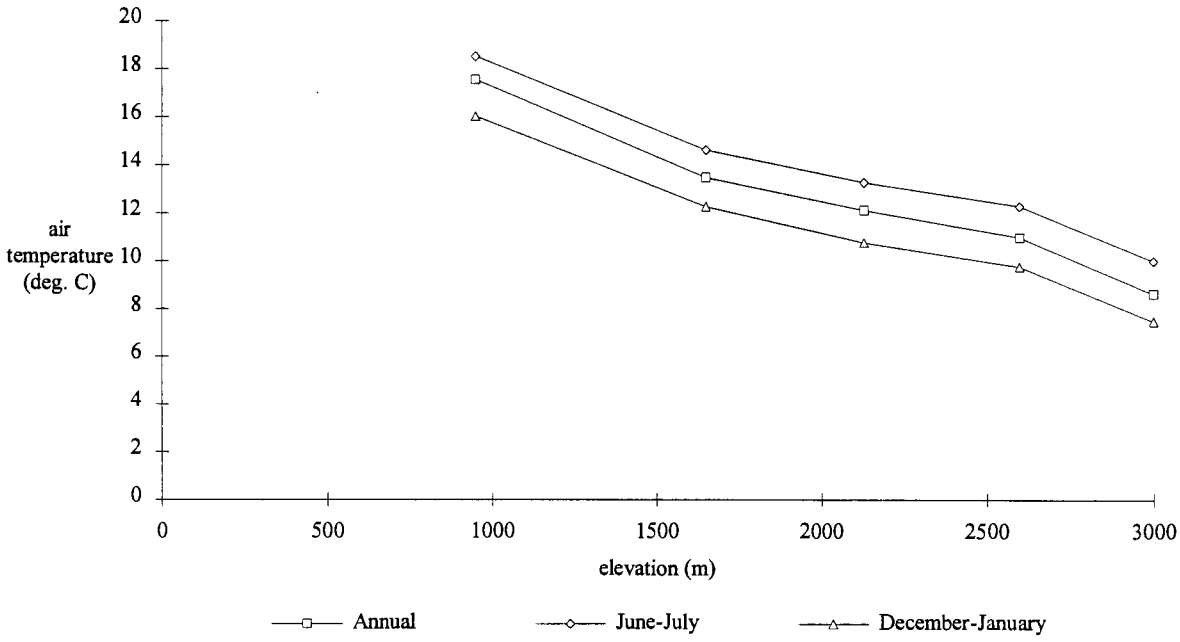

Figure 15 - Mean Air Temperature

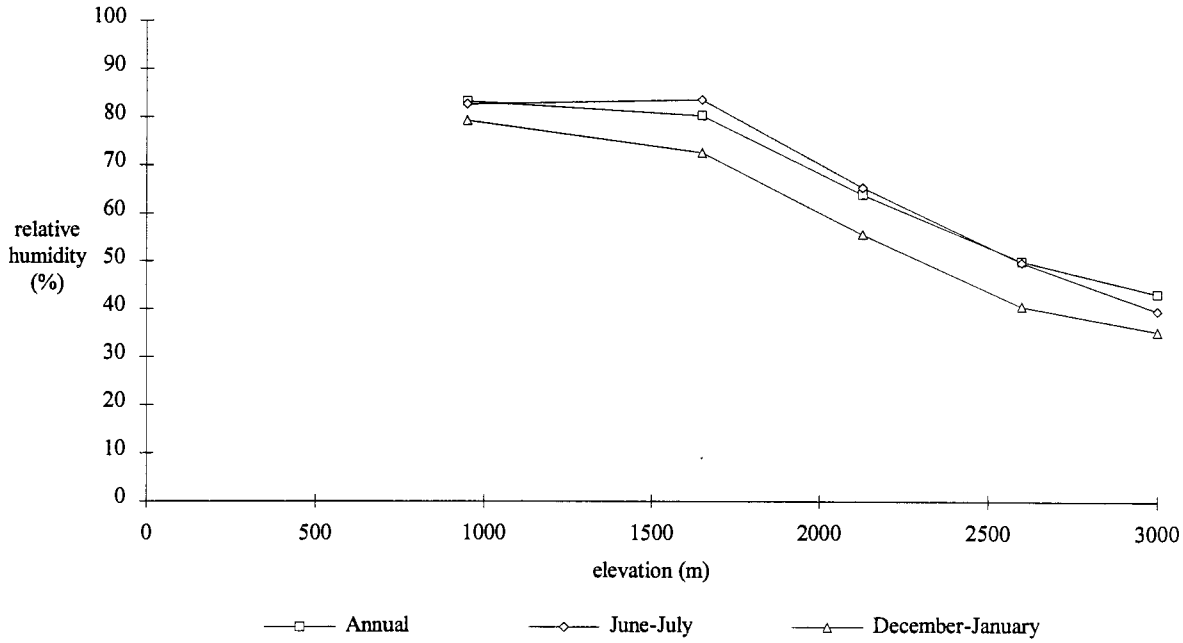

Figure 16 - Mean Relative Humidity

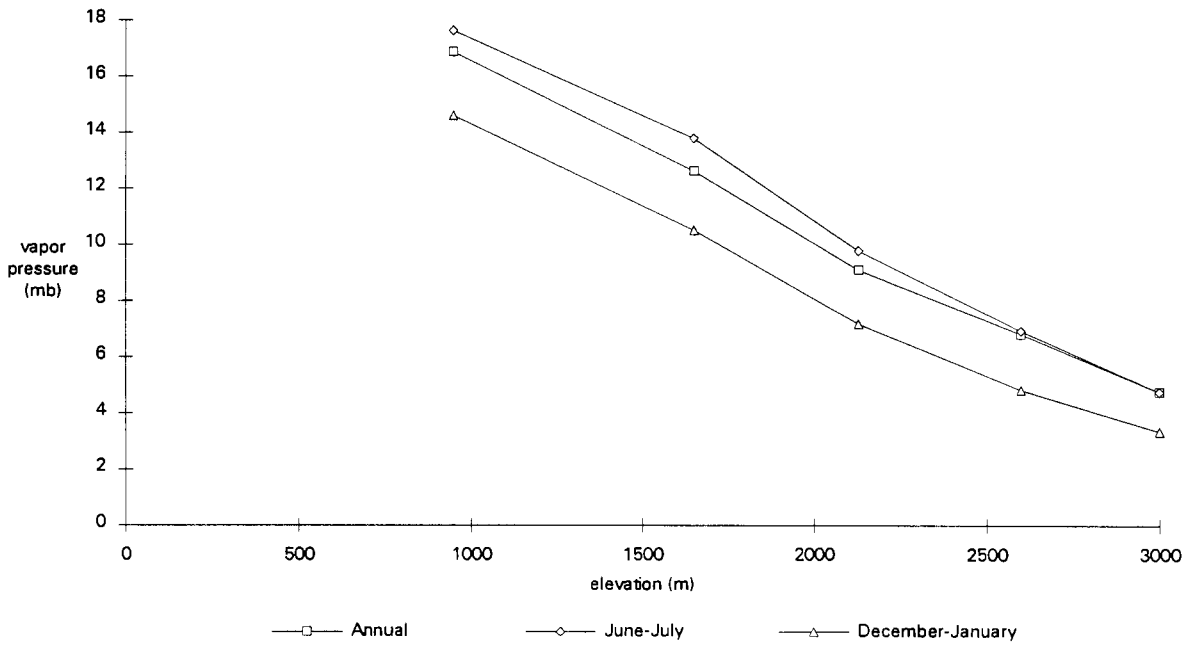

Figure 17 - Mean Vapor Pressure

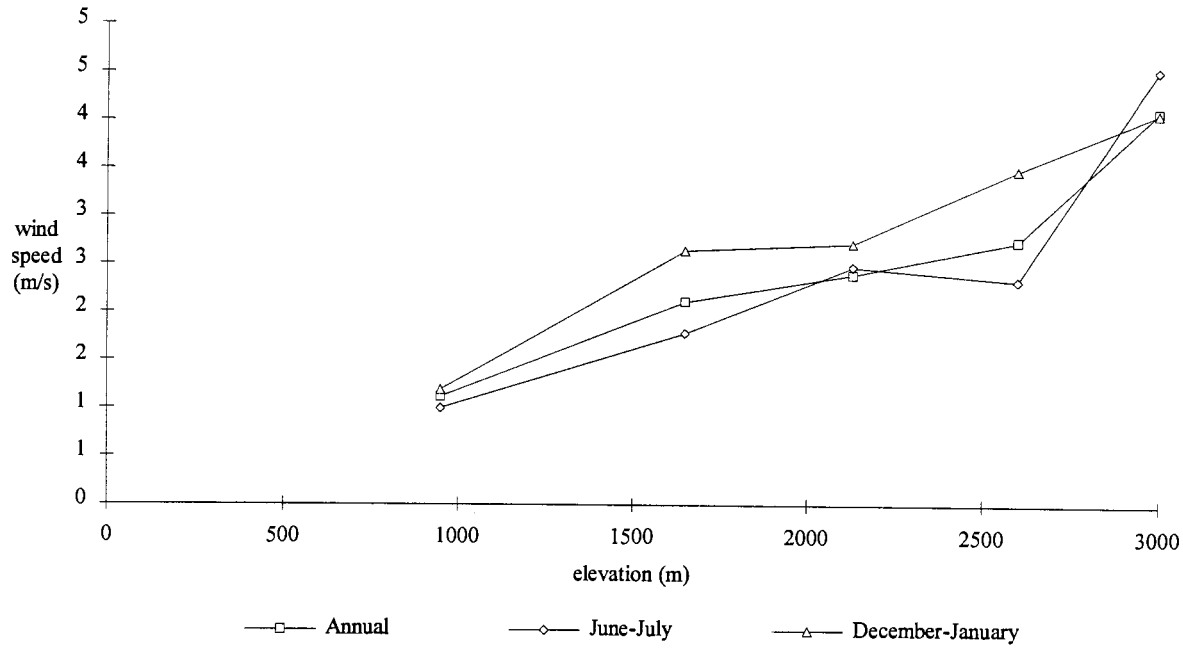

Figure 18 - Mean Wind Speed

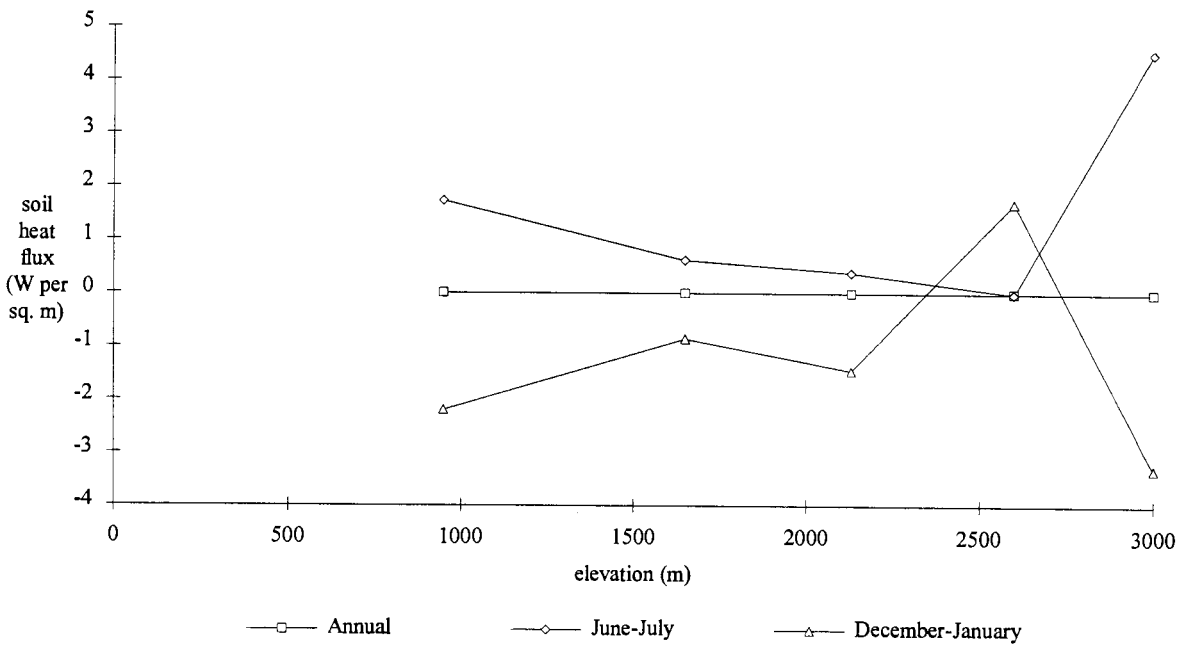

Figure 19 - Mean Soil Heat Flux

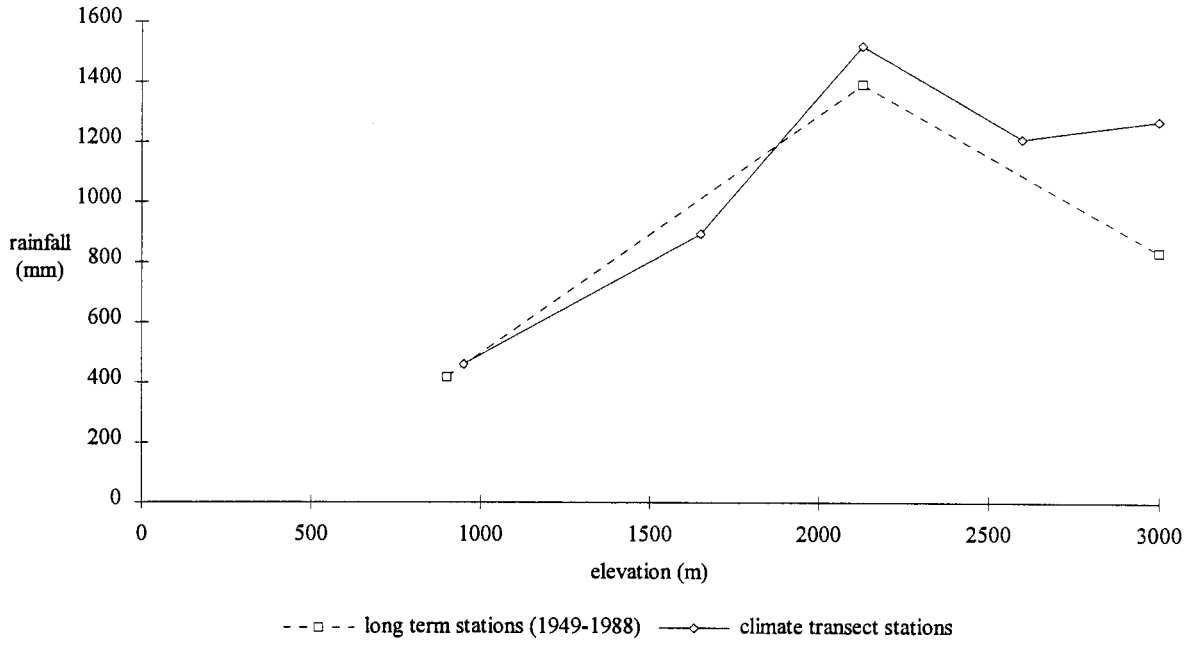

Figure 20 - Annual Mean Rainfall

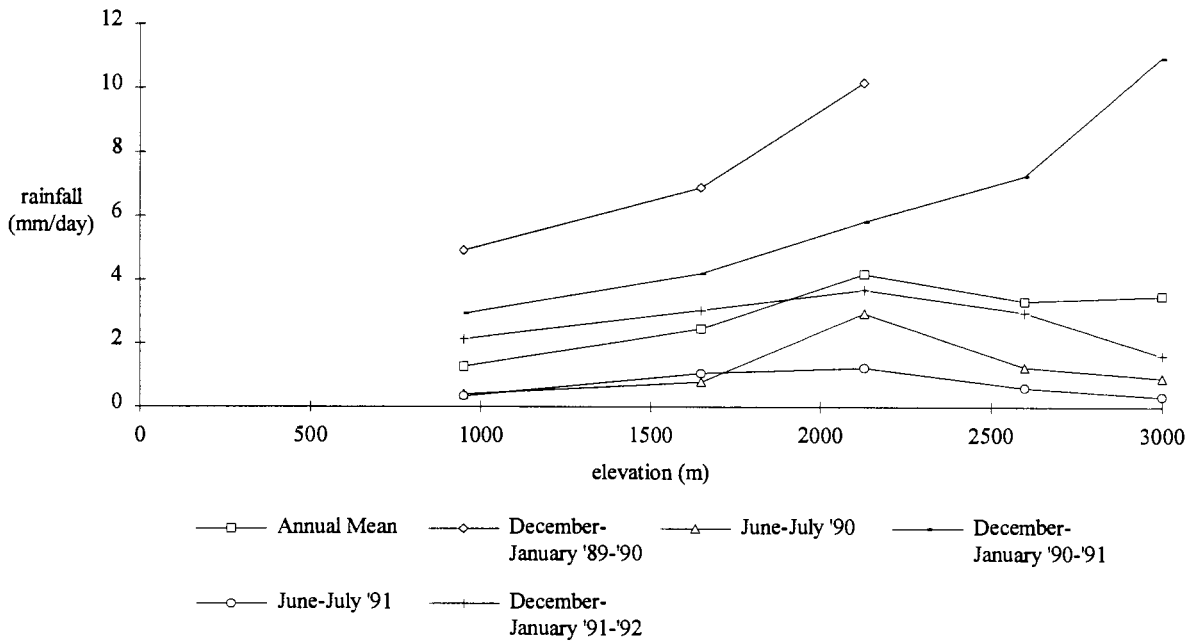

Figure 21 - Seasonal and Annual Rainfalll Along Cllimate Station Transect

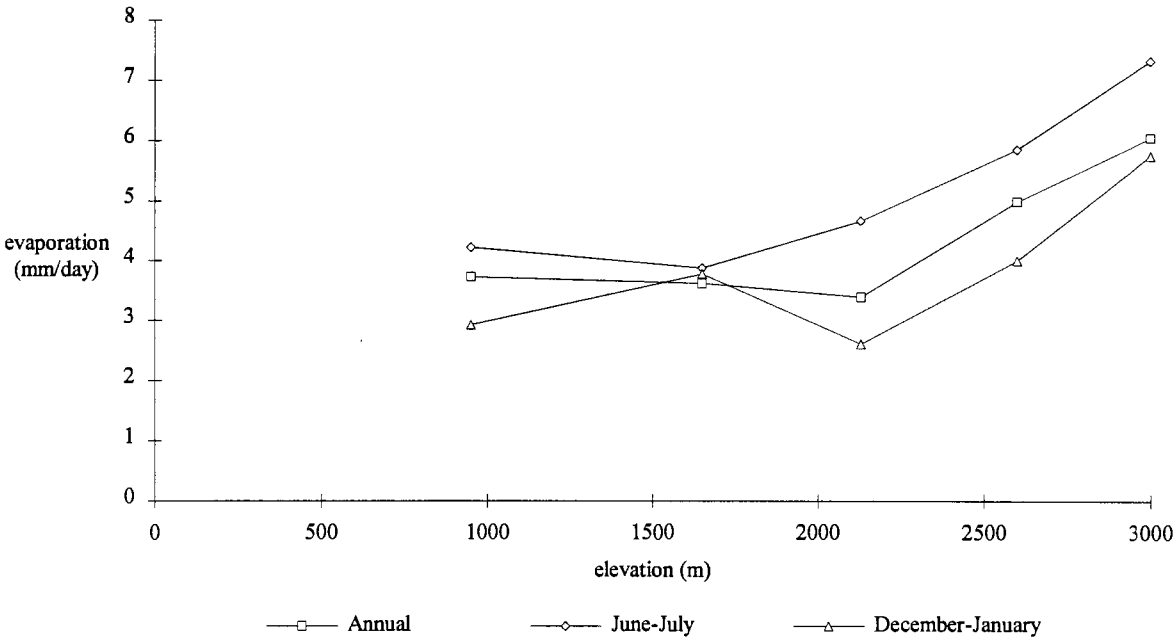

Figure 22 - Annual Mean Atmometer Evaporation

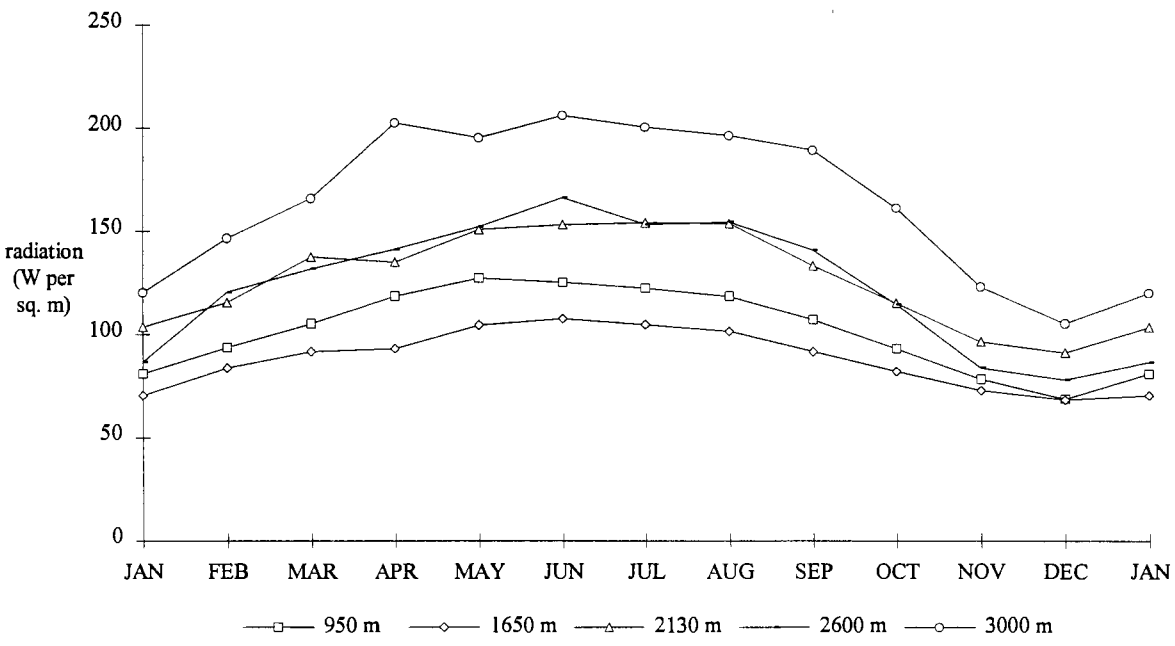

Figure 23 - Annual Cycle of Net Radiation

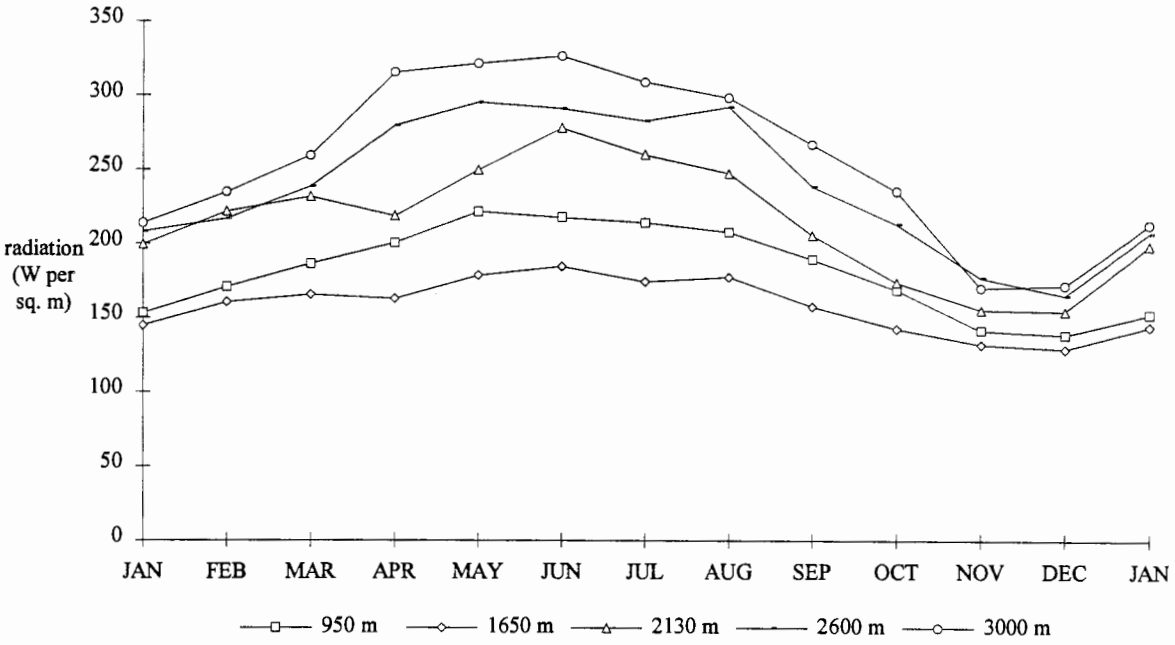

Figure 24 - Annual Cycle of Global Radiation

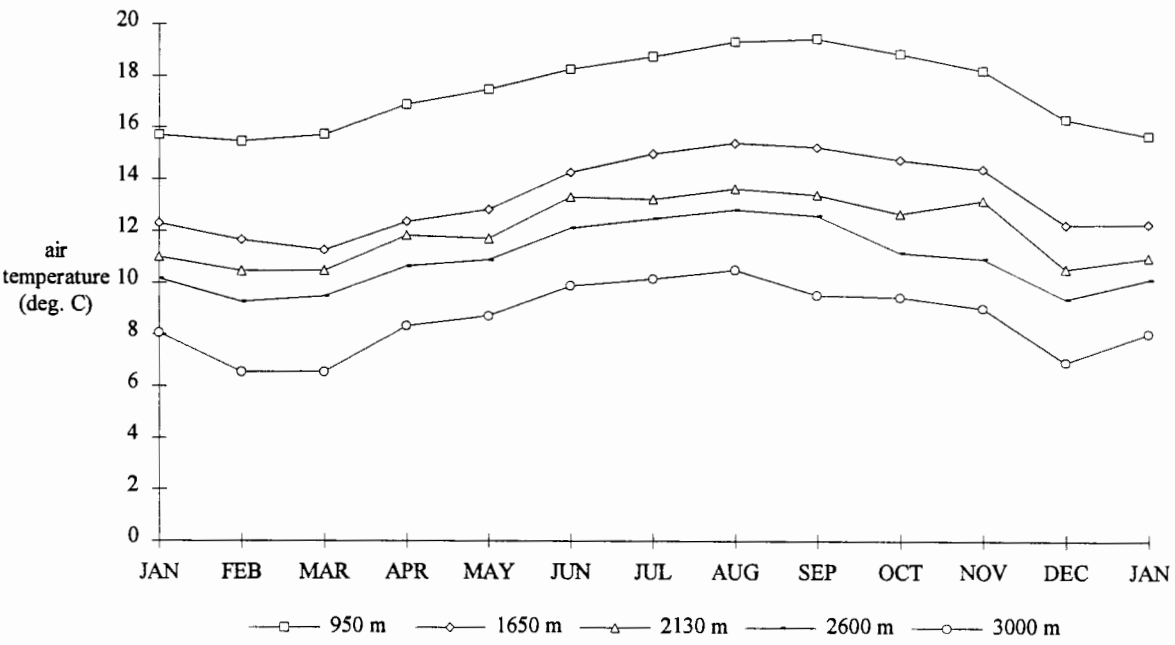

Figure 25 - Annual Cycle of Air Temperature

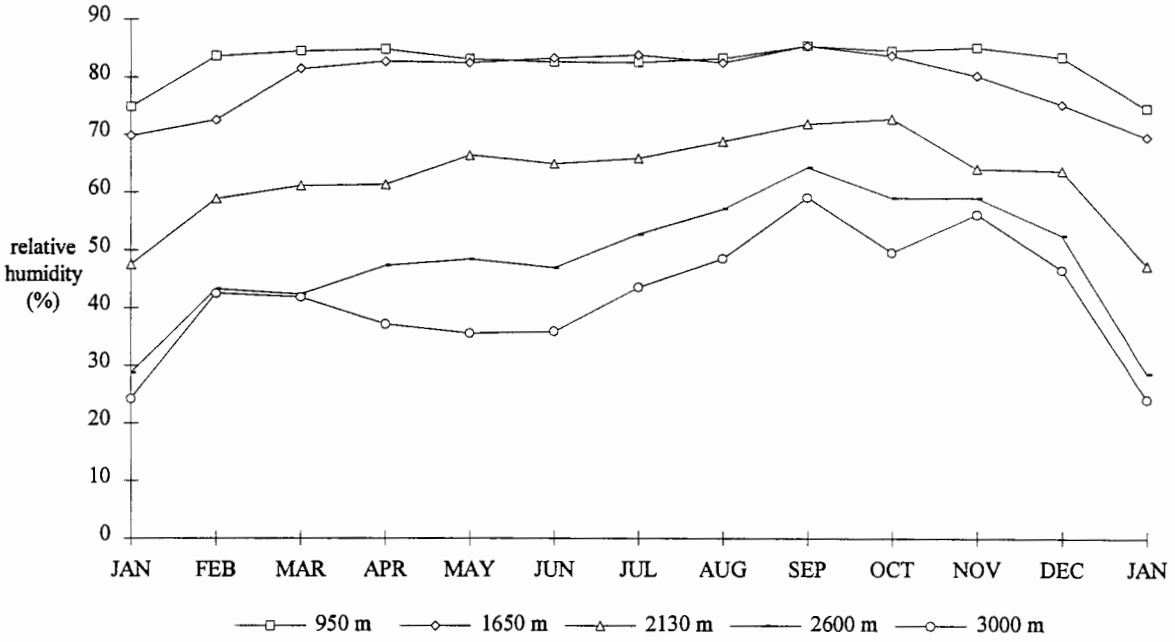

Figure 26 - Annual Cycle of Relative Humidity

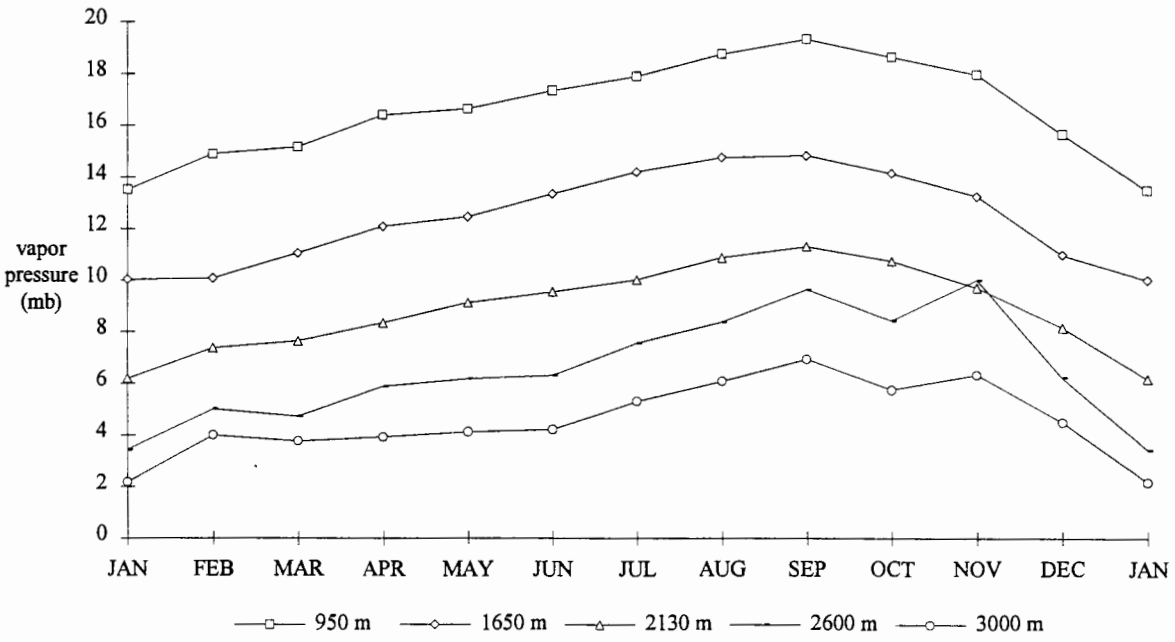

Figure 27 - Annual Cycle of Vapor Pressure

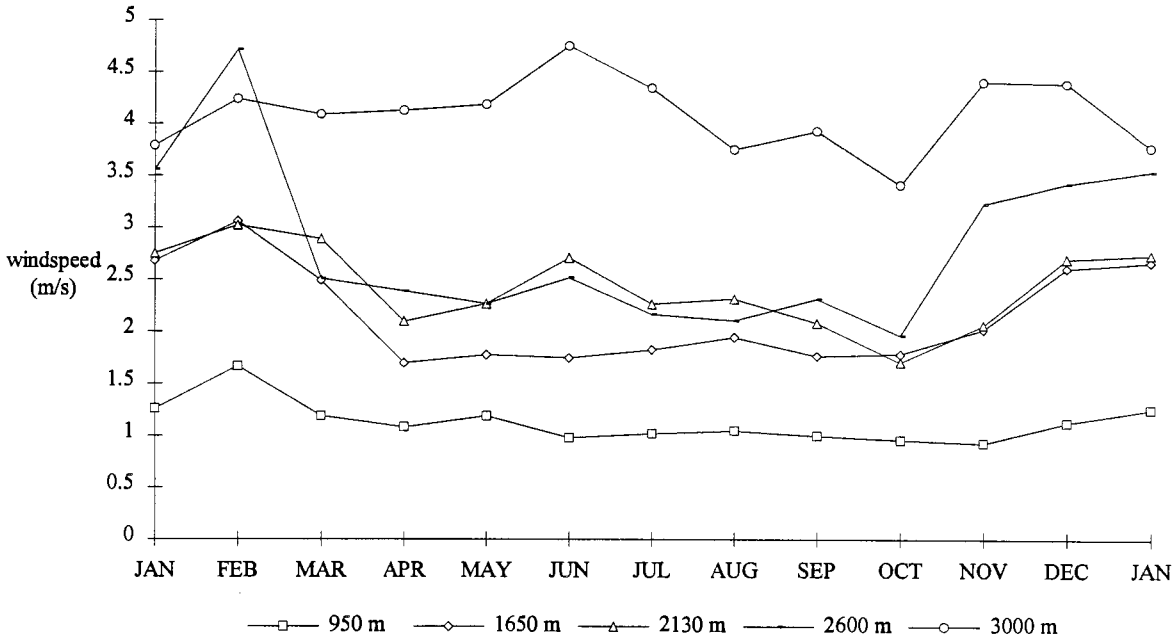

Figure 28 - Annual Cycle of Windspeed

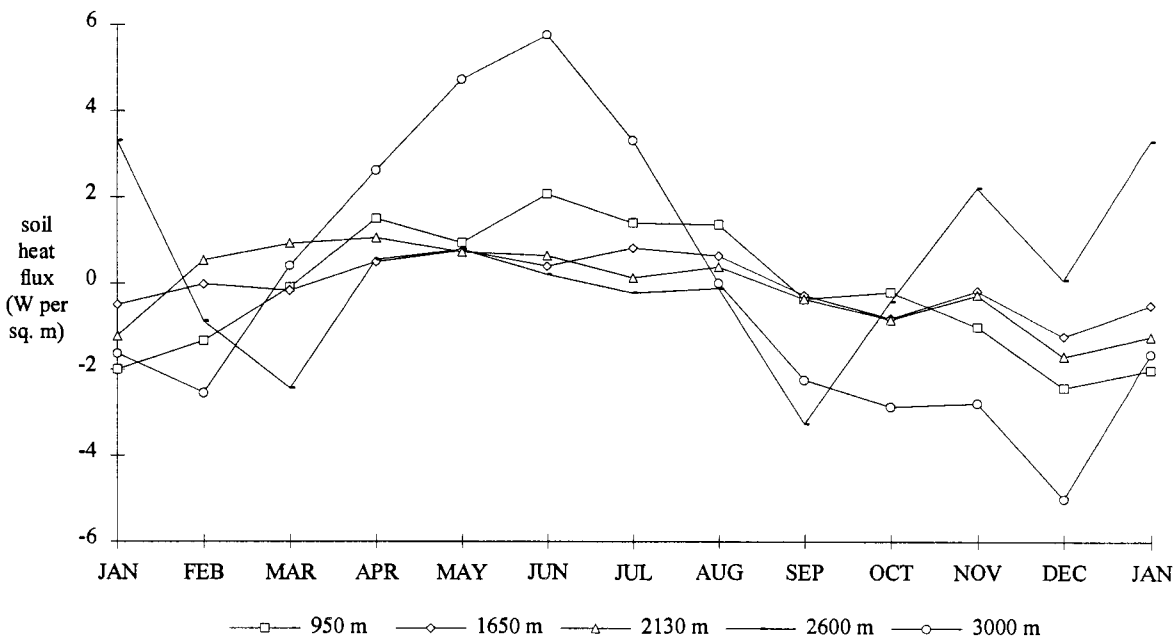

Figure 29 - Annual Cycle of Soil Heat Flux

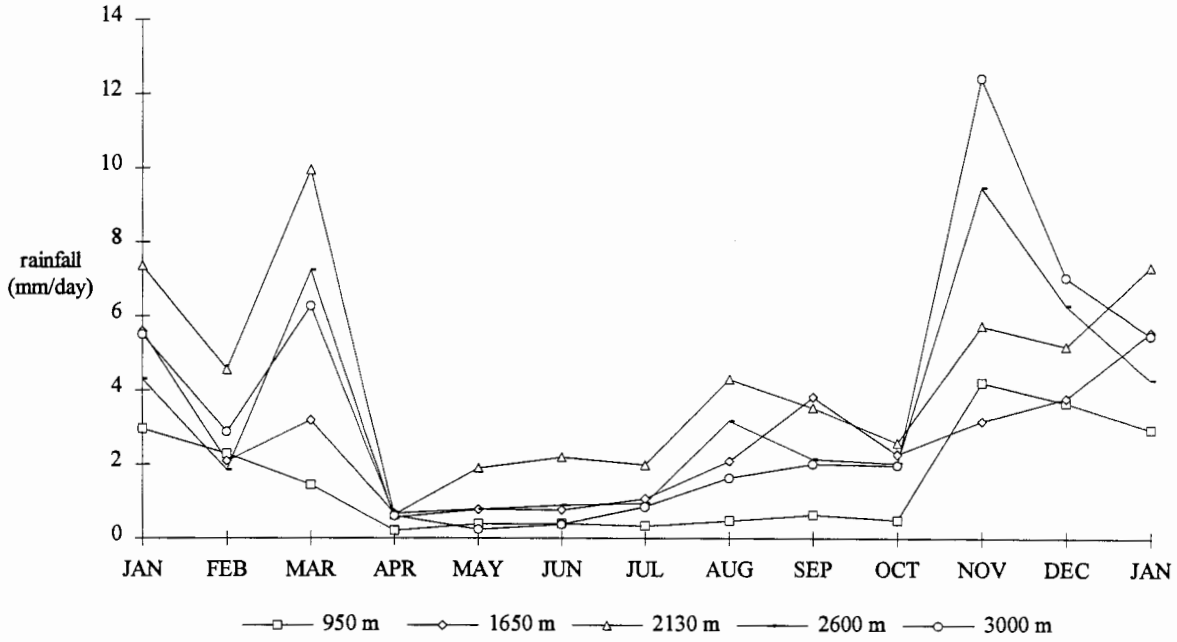

Figure 30 - Annual Cycle of Rainfall

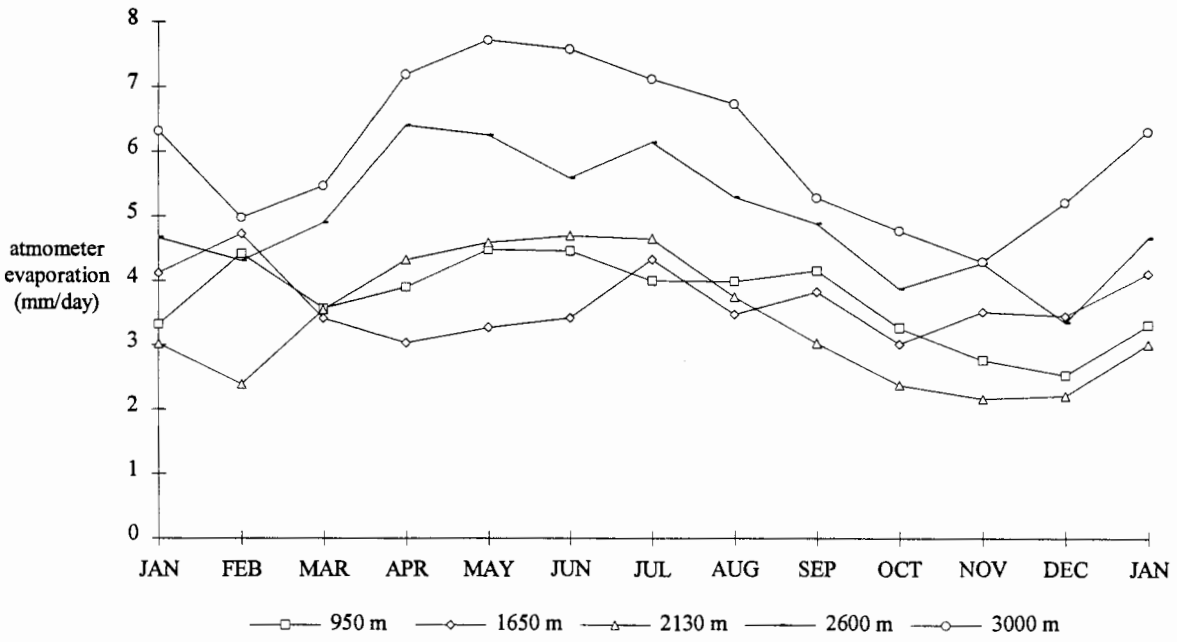

Figure 31 - Annual Cycle of Atmometer Evaporation

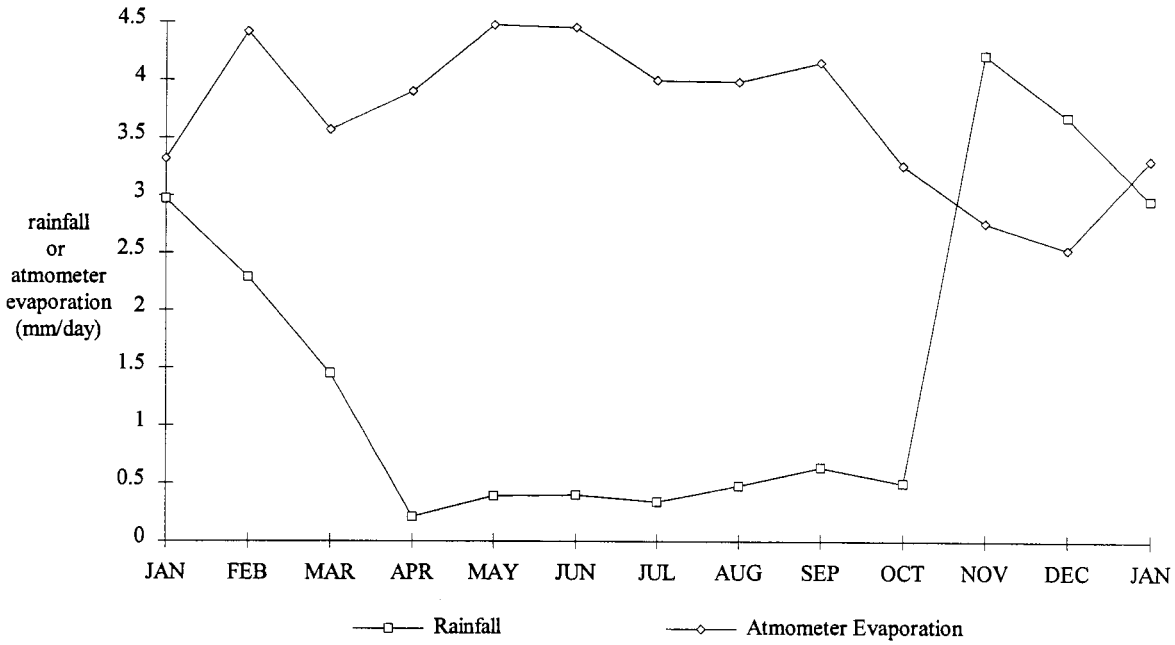

Figure 32 - Annual Cycle of Rainfall Versus Atmometer Evaporation at 950 meters Elevation

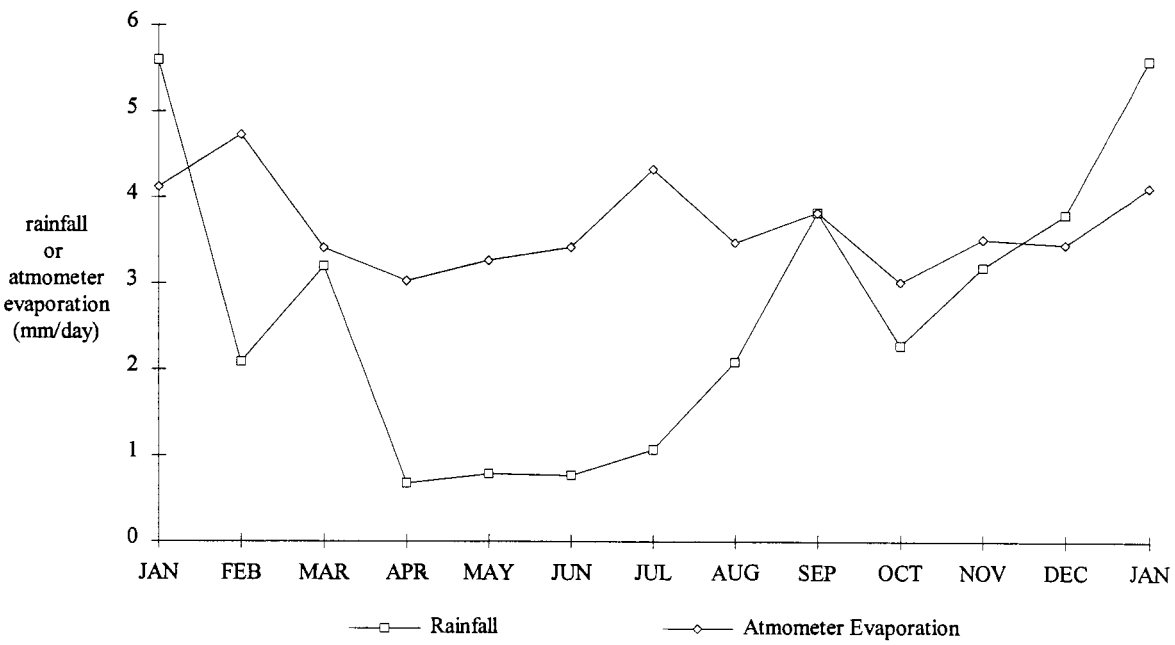

Figure 33 - Annual Cycle of Rainfall Versus Atmometer Evaporation at 1650 meters Elevation

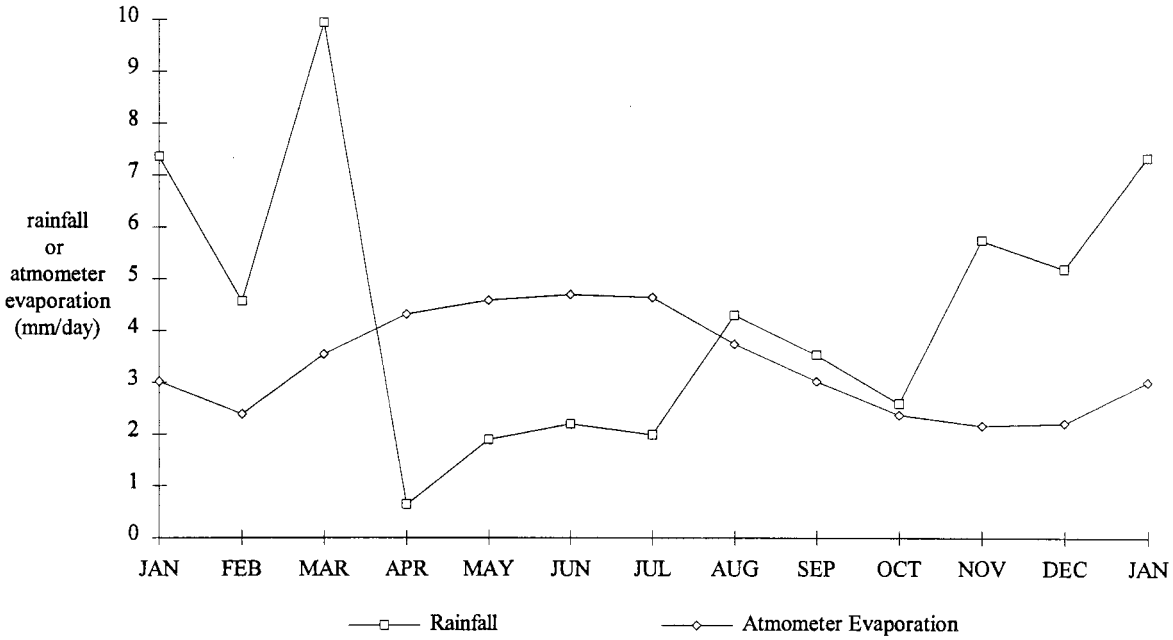

Figure 34 - Annual Cycle of Rainfall Versus Atmometer Evaporation at 2130 meters Elevation

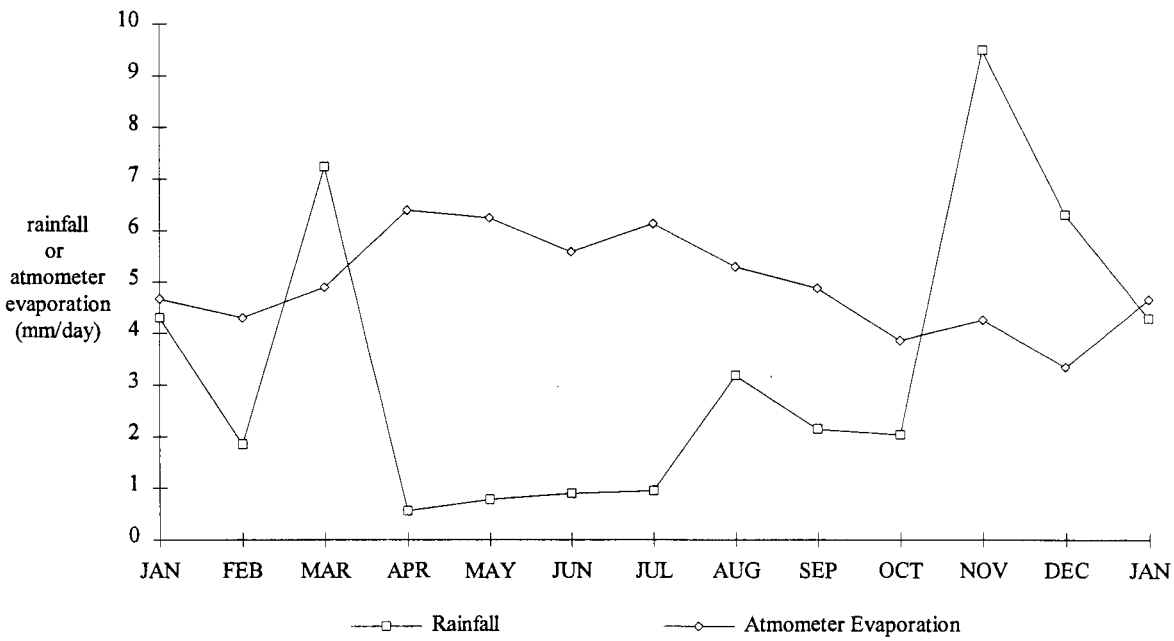

Figure 35 - Annual Cycle of Rainfall Versus Atmometer Evaporation at 2600 meters Elevation

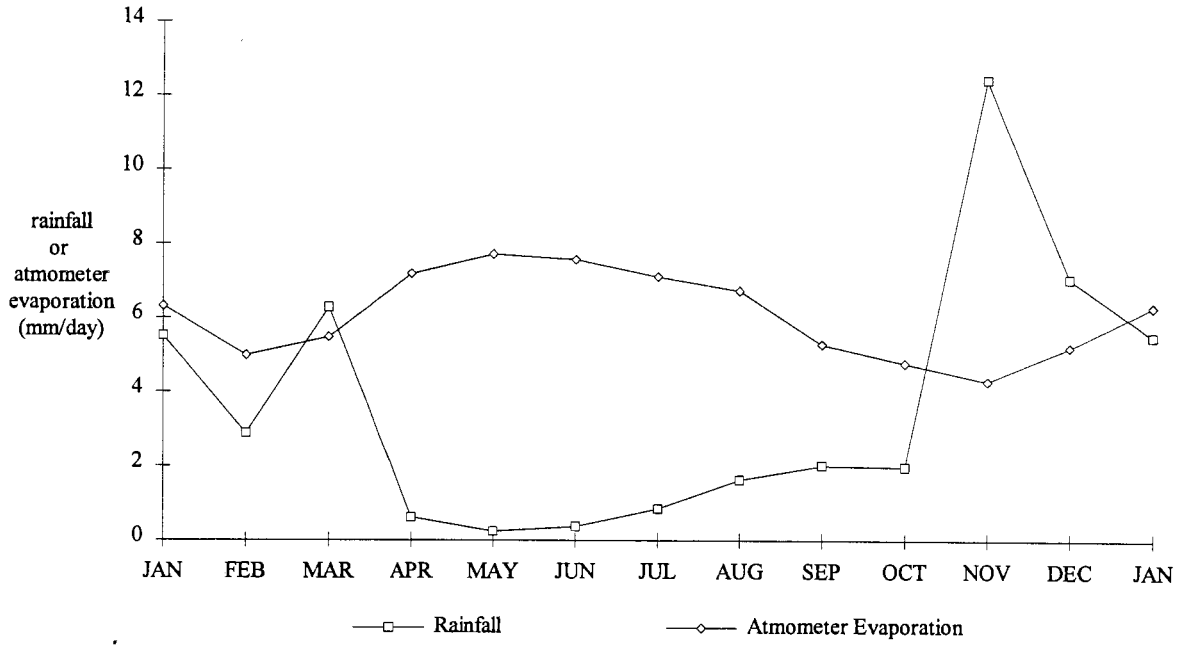

Figure 36 - Annual Cycle of Rainfall Versus Atmometer Evaporation at 3000 meters Elevation

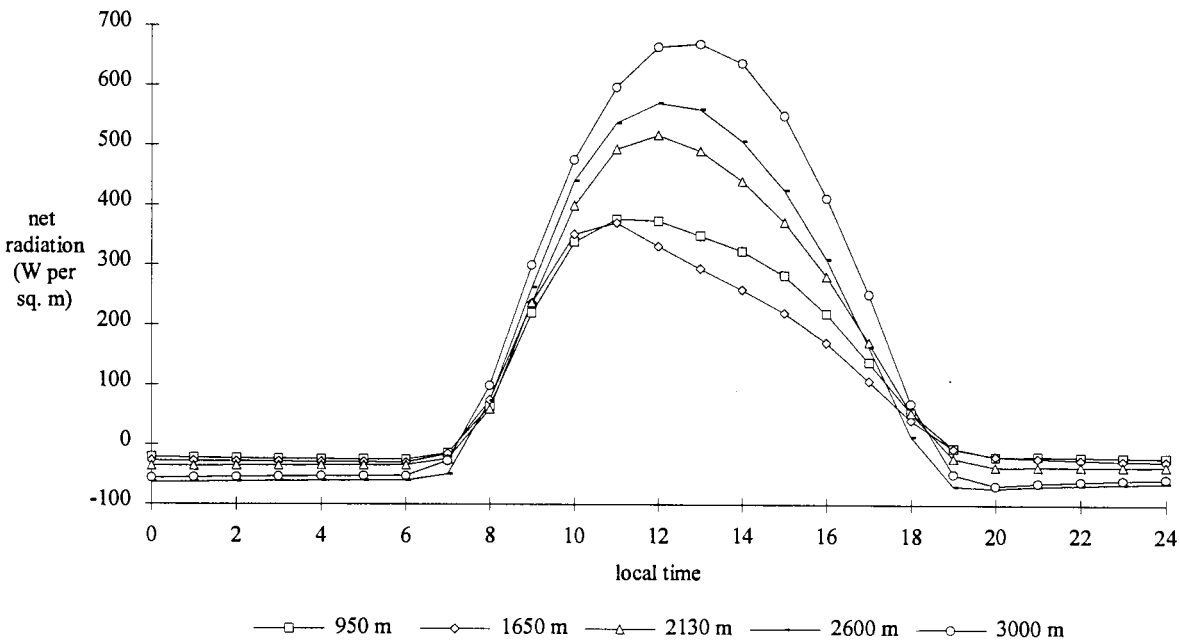

Figure 37 - Mean Diurnal Cycle of Net Radiation

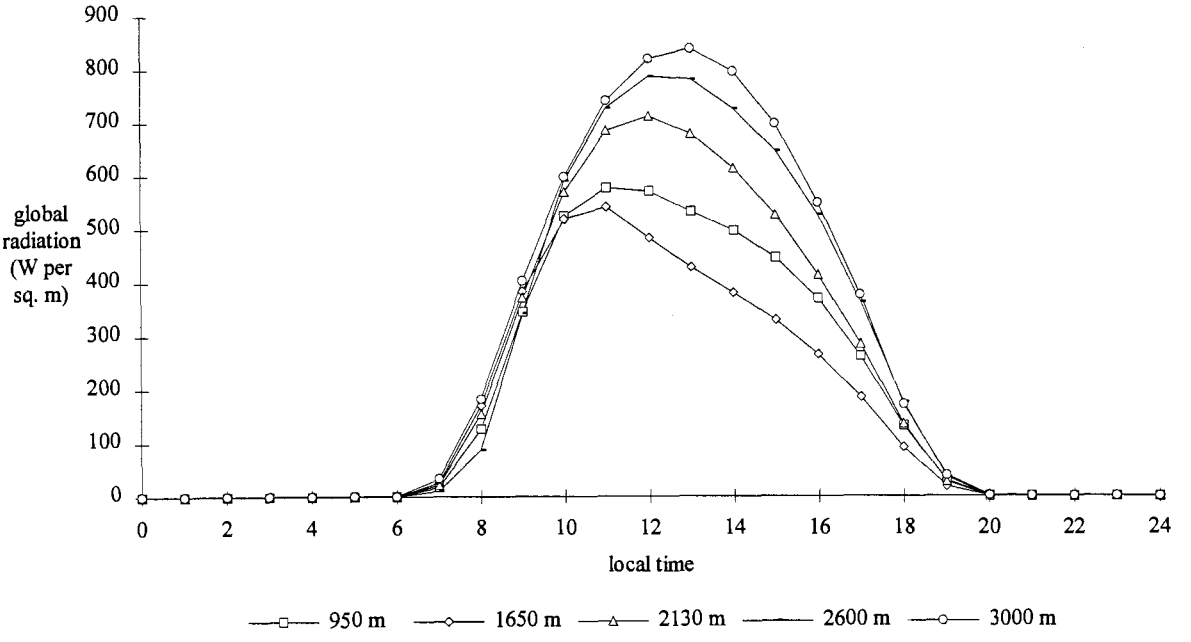

Figure 38 - Mean Diurnal Cycle of Global Radiation

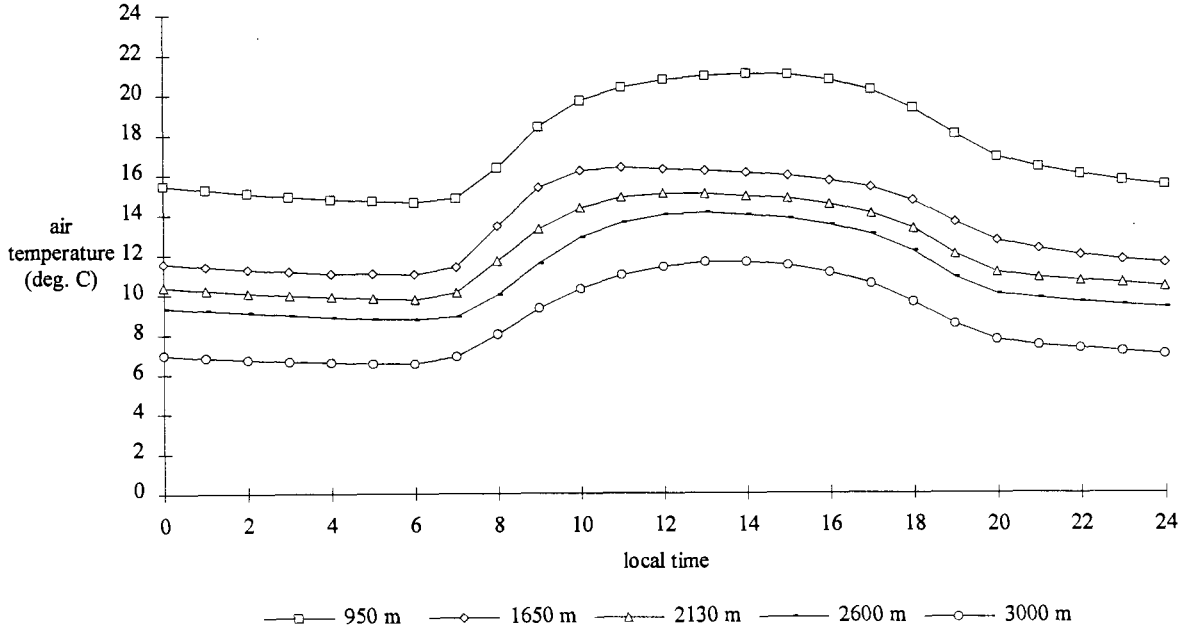

Figure 39 - Mean Diurnal Cycle of Air Temperature

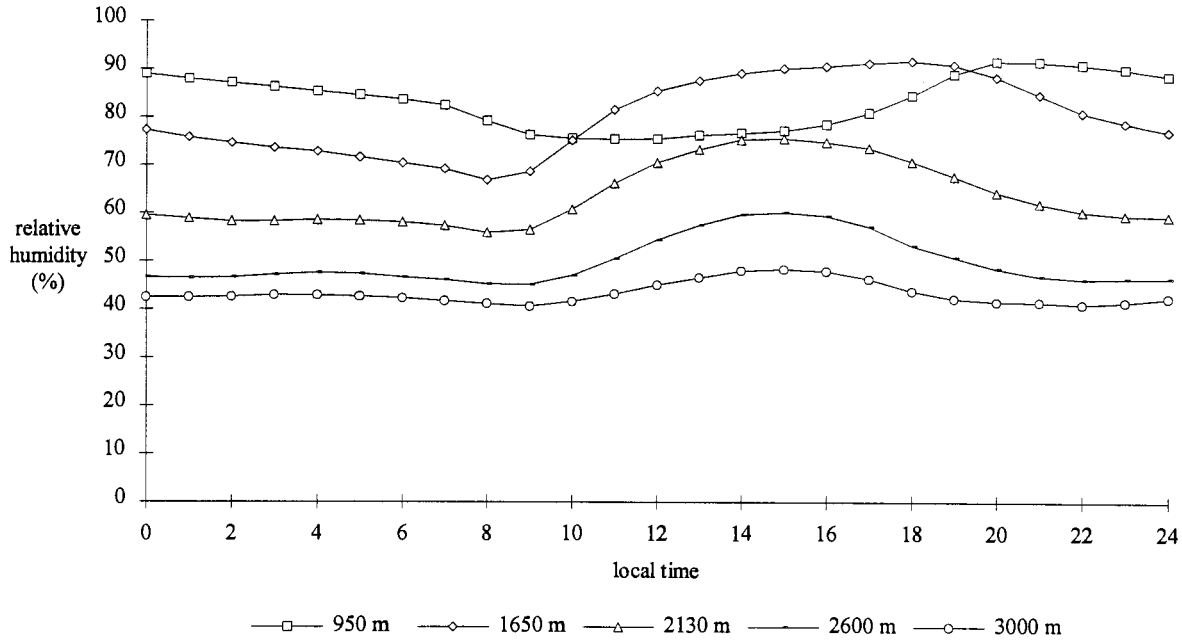

Figure 40 - Mean Diurnal Cycle of Relative Humidity

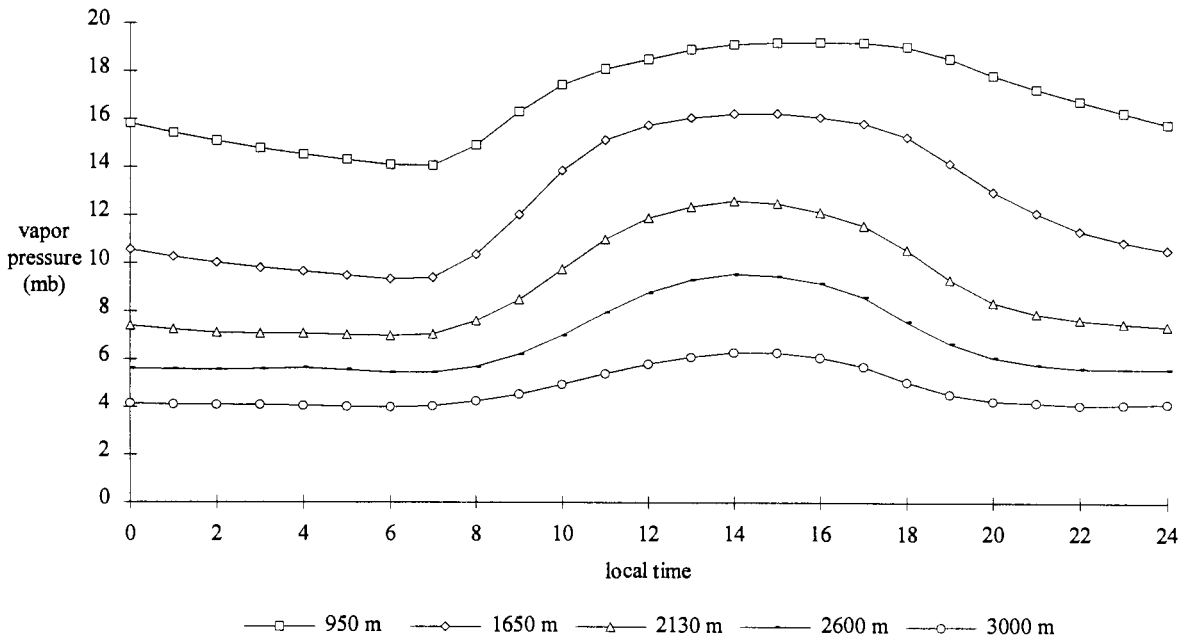

Figure 41 - Mean Diurnal Cycle of Vapor Pressure

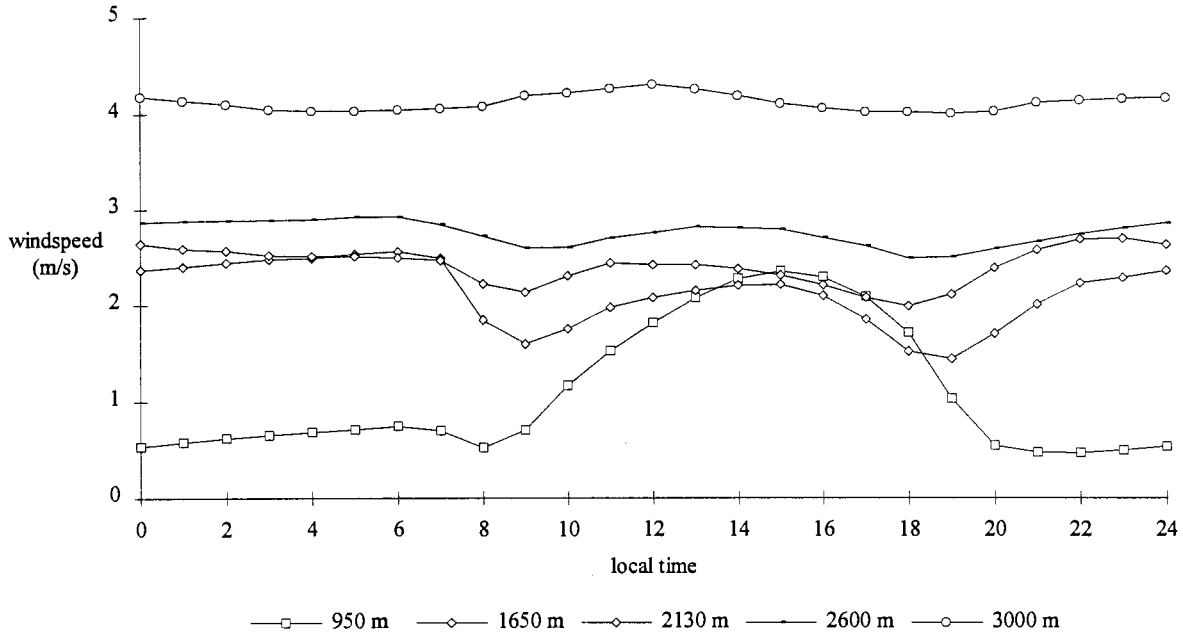

Figure 42 - Mean Diurnal Cycle of Windspeed

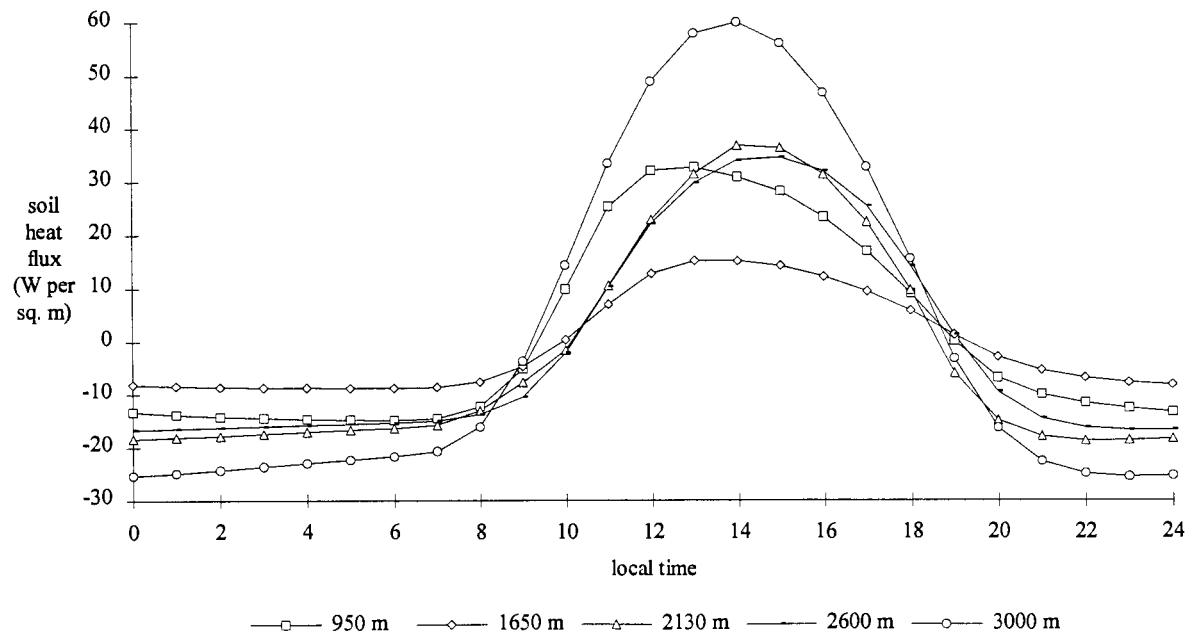

Figure 43 - Mean Diurnal Cycle of Soil Heat Flux

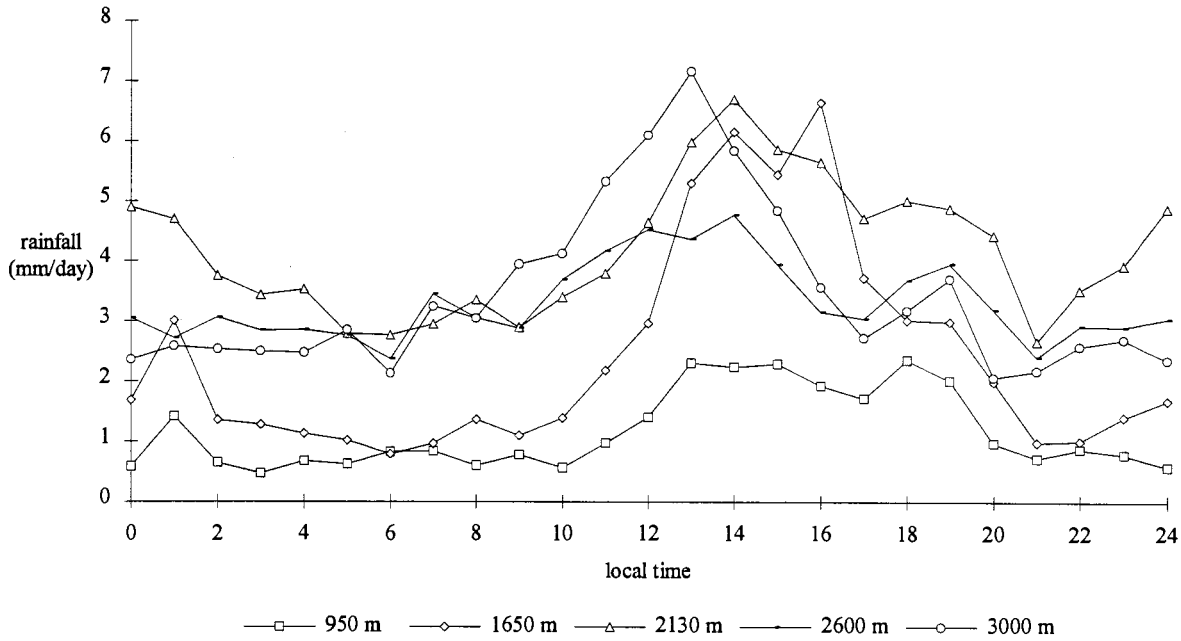

Figure 44 - Mean Diurnal Cycle of Rainfall

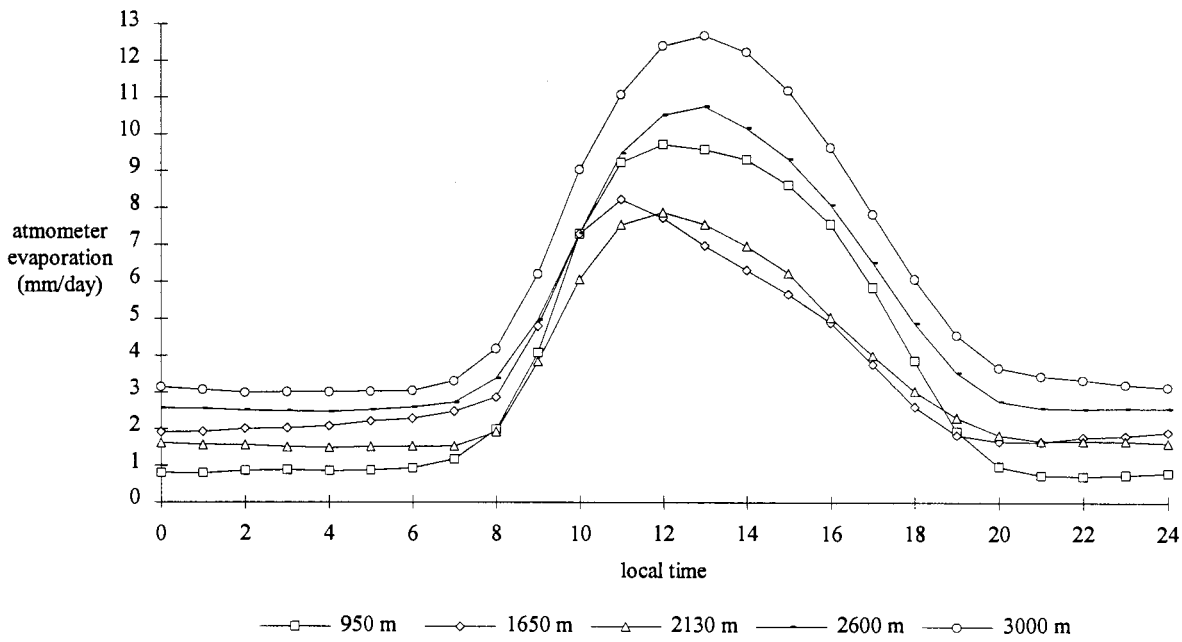

Figure 45 - Mean Diurnal Cycle of Atmometer Evaporation

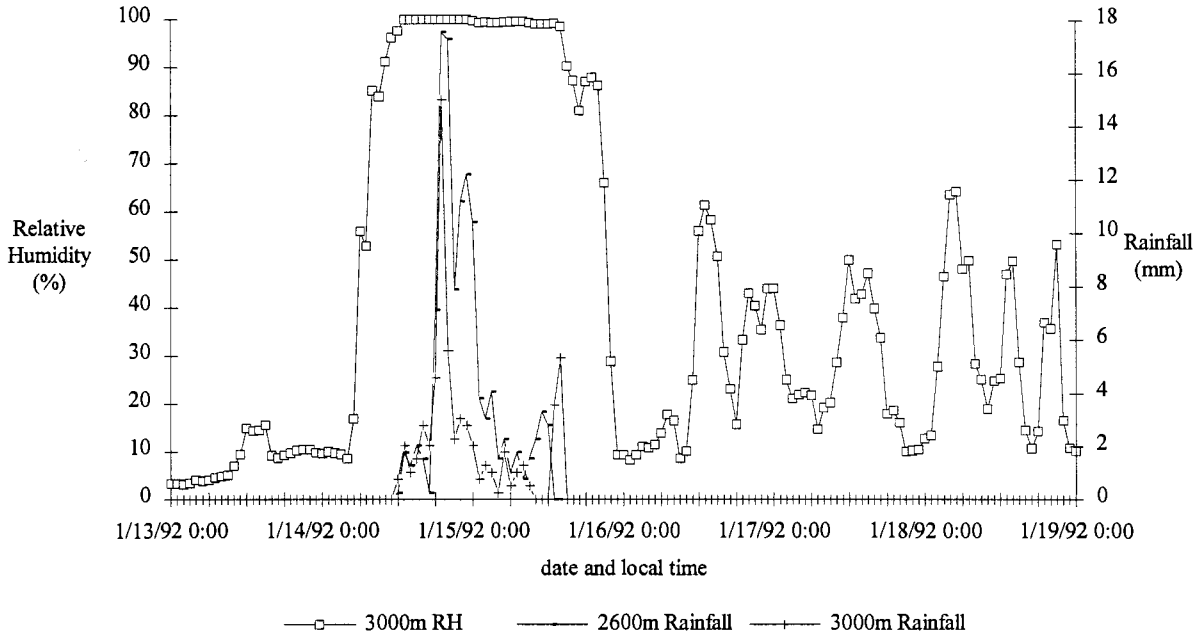

Figure 46 - Relative Humidity and Rainfall During Snowstorm of January 14-15, 1992

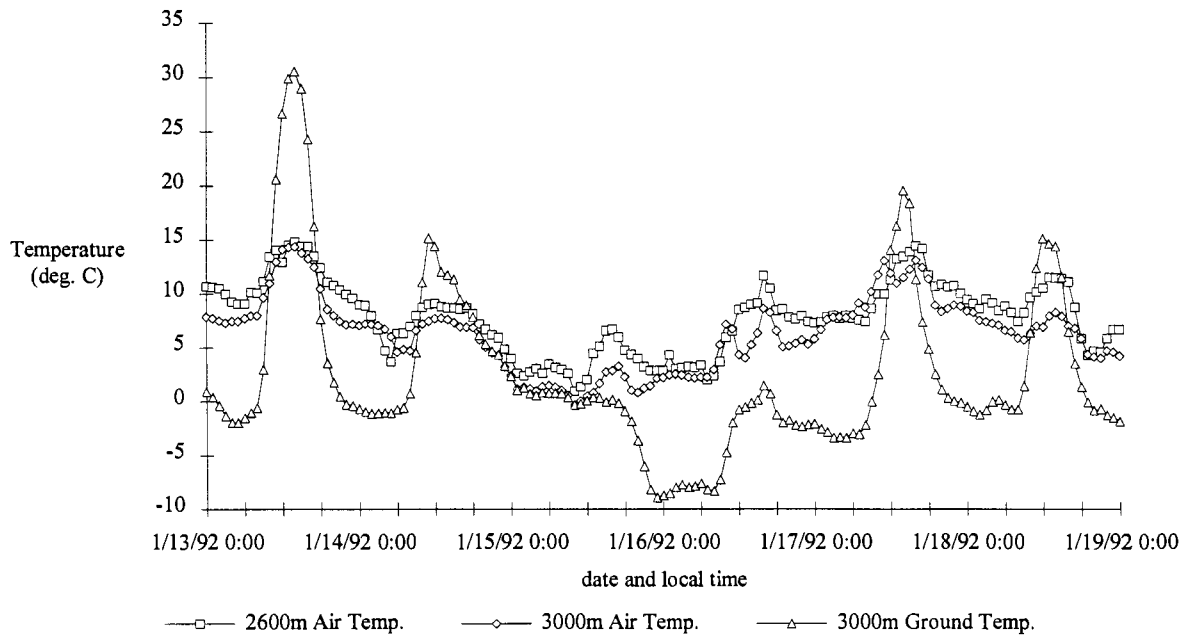

Figure 47 - Air and Ground Temperatures During Snowstorm of January 14-15, 1992

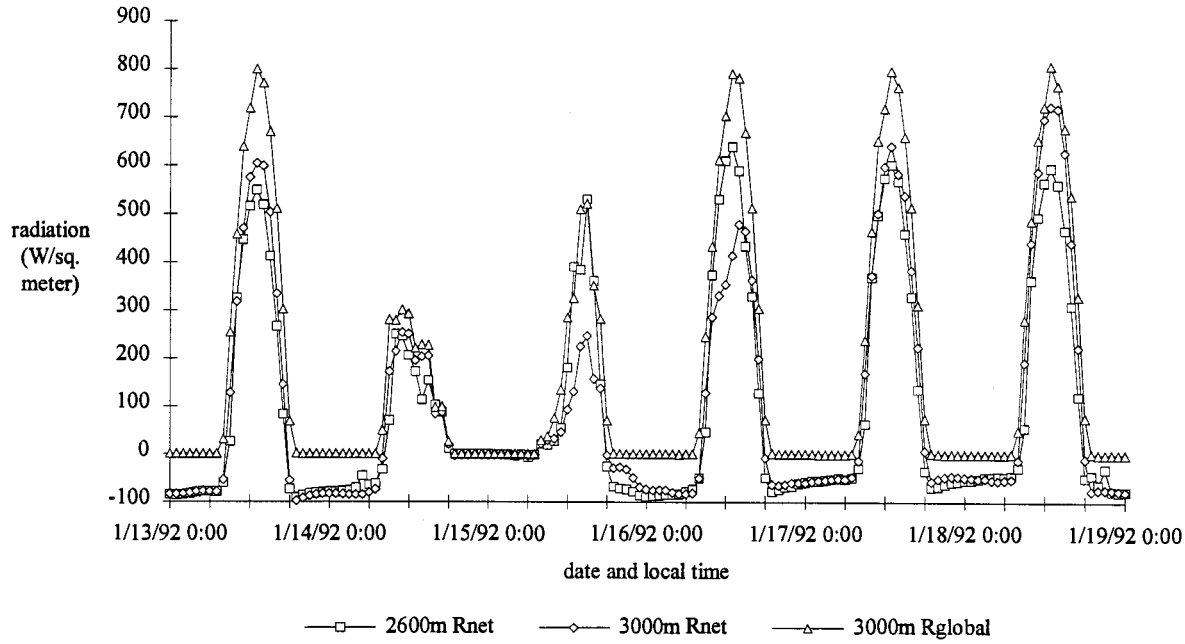

Figure 48 - Net and Global Radiation During Snowstorm of January 14-15, 1992

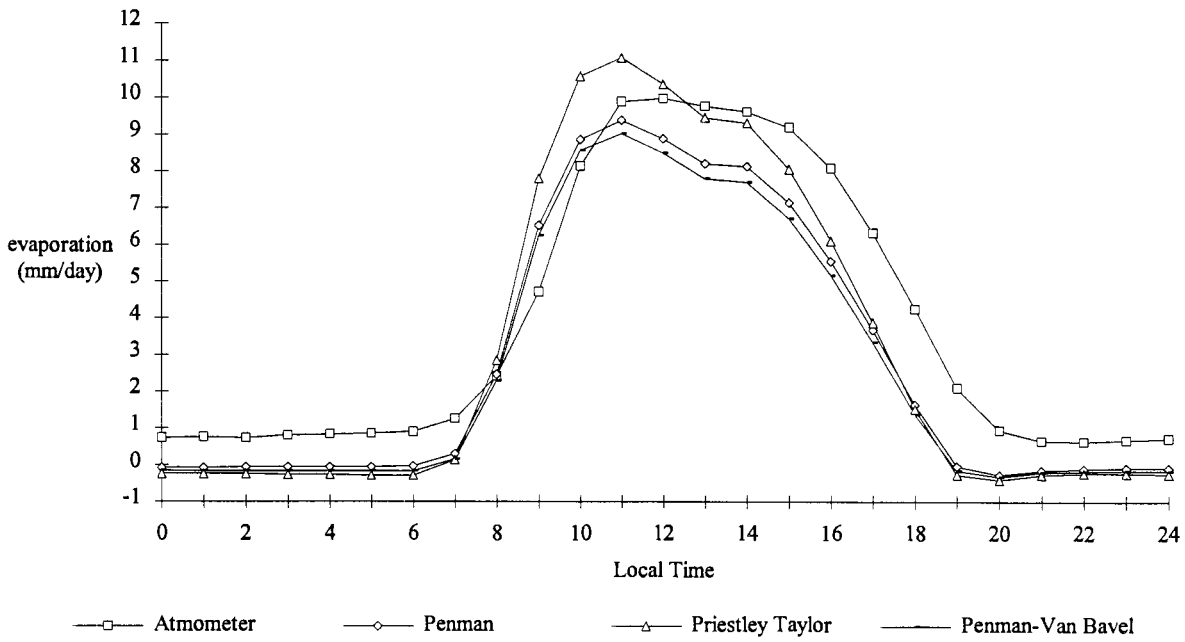

Figure 49 - Diurnal Pattern of Atmometer Measurements Versus Potential Evaporation Estimates at 950 meters Elevation

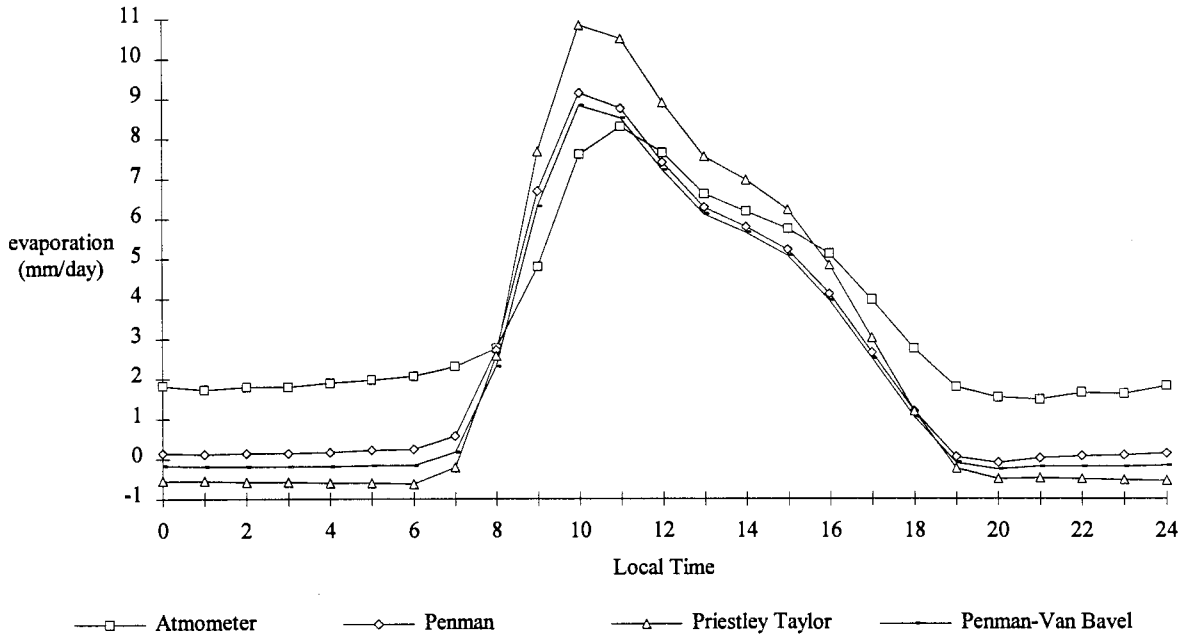

Figure 50 - Diurnal Pattern of Atmometer Measurements Versus Potential Evaporation Estimates at 1650 meters Elevation

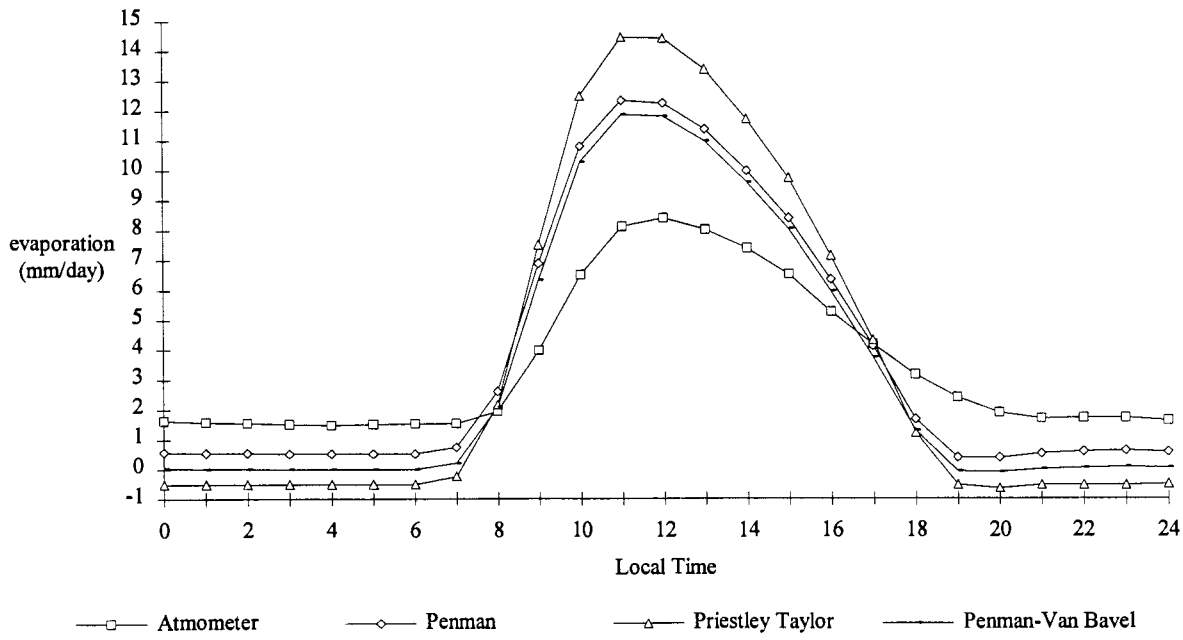

Figure 51 - Diurnal Pattern of Atmometer Measurements Versus Potential Evaporation Estimates at 2130 meters Elevation

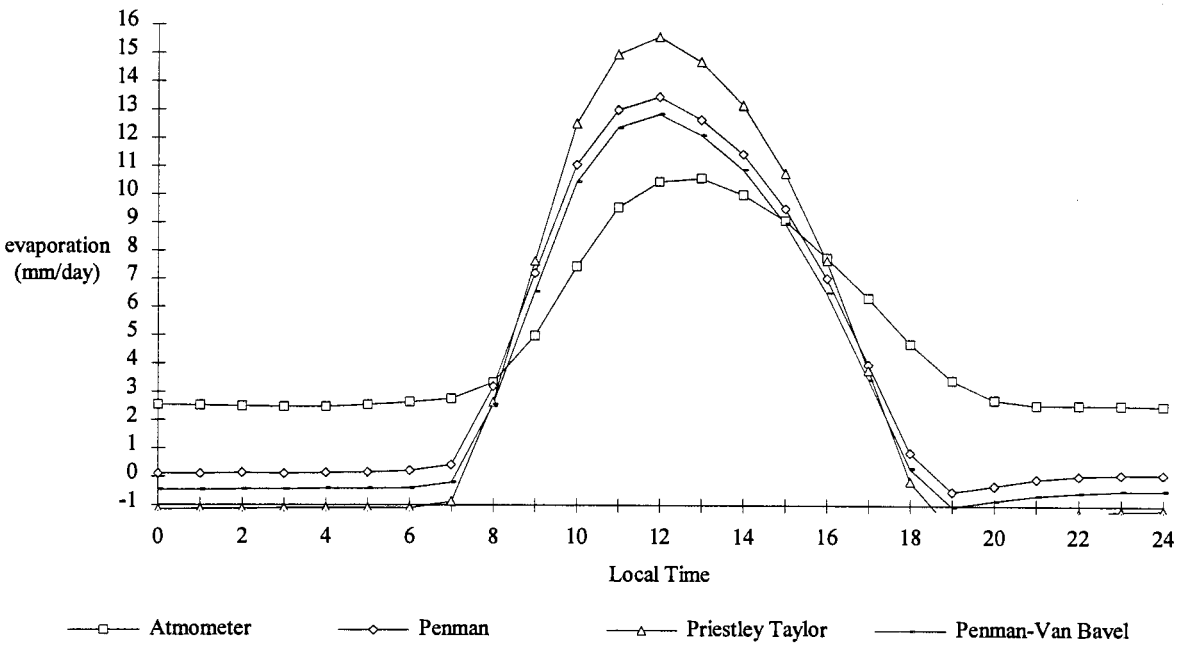

Figure 52 - Diurnal Pattern of Atmometer Measurements Versus Potential Evaporation Estimates at 2600 meters Elevation

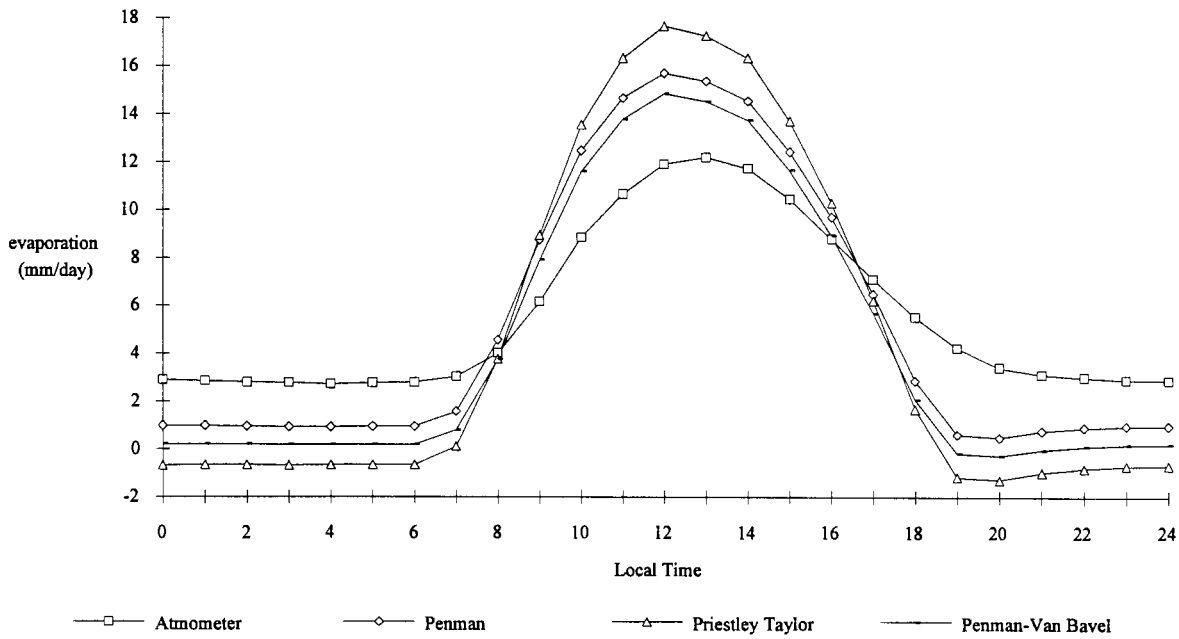

Figure 53 - Diurnal Pattern of Atmometer Measurements Versus Potential Evaporation Estimates at 3000 meters Elevation